Publicly Accessible Penn Dissertations

2022

# The Role Of Neuropilin2a/b And Sema3fa In The Protoglomerular Targeting Of Zebrafish Olfactory Sensory Neurons

Ryan Pei-Yen Cheng
*University of Pennsylvania*

# The Role Of Neuropilin2a/b And Sema3fa In The Protoglomerular Targeting Of Zebrafish Olfactory Sensory Neurons

## Abstract

During development, zebrafish olfactory sensory neurons (OSNs) project axons from the olfactory epithelium to neuropil structures in the olfactory bulb (OB) known as protoglomeruli. OSNs expressing either OMP or TRPC2 exclusively project axons to two distinct, complementary sets of protoglomeruli. It is not known how differential protoglomerular targeting of these two populations is maintained. The guidance receptors nrp2a and nrp2b, along with their ligand sema3fa, were identified through RNAseq as potential candidates responsible for differential protoglomerular targeting of OMP- and TRPC2-class OSNs. Nrp2a and nrp2b are expressed in TRPC2-class OSNs, while sema3fa is expressed in OMP-class OSNs and OB. To investigate the involvement of these guidance factors in OSN axon guidance, the protoglomerular targeting fidelity of OSNs expressing OMP:RFP or TRPC2:Venus were assessed in nrp2a, nrp2b, and sema3fa mutants. The roles for these three guidance factors were further investigated through genetic interaction studies and live time-lapse imaging experiments. Targeting fidelity of TRPC2-class OSNs is degraded in nrp2a, nrp2b, and sema3fa mutants with increased rates of misprojecting axons observed in OMP-specific protoglomeruli as well as non-protoglomerular regions within the OB. Genetic interaction experiments suggest that nrp2a and nrp2b are partially redundant and that sema3fa is likely one of multiple guidance cues that acts in the same pathway as nrp2a and nrp2b. Live time-lapse imaging experiments comparing nrp2a and sema3fa mutants to their heterozygous siblings show that the dynamic behavior of TRPC2-class OSN growth cones are altered in mutant animals. The results support a model in which sema3fa functions as a repulsive cue to exclude nrp2a- and/or nrp2b-expressing TRPC2-class OSNs from OMP-specific protoglomeruli as well as form the dorsal-medial OB, adding to a growing list of guidance factors involved in protoglomerular targeting of OSNs. I also describe a protocol for the registration of guidance cue expression data in the 36hpf OB and present an unbiased registration template and model of the 72hpf OB and protoglomeruli. This work highlights the complex interaction of guidance factors involved in protoglomerular targeting of OSNs and lays a foundation for the systematic study of olfactory circuit formation.

## Degree Type
Dissertation

## Degree Name
Doctor of Philosophy (PhD)

## Graduate Group
Cell & Molecular Biology

## First Advisor
Jonathan A. Raper

## Keywords
Axon guidance, Live imaging, Olfactory sensory neuron, Protoglomerulus, Zebrafish

## Subject Categories
Developmental Biology | Neuroscience and Neurobiology

THE ROLE OF NEUROPILIN2A/B AND SEMA3FA IN THE PROTOGLOMERULAR TARGETING

OF ZEBRAFISH OLFACTORY SENSORY NEURONS

Ryan Pei-Yen Cheng

A DISSERTATION

in

Cell and Molecular Biology

Presented to the Faculties of the University of Pennsylvania

in

Partial Fulfillment of the Requirements for the

Degree of Doctor of Philosophy

2022

Supervisor of Dissertation

Jonathan A. Raper, Ph.D.

Professor of Neuroscience


Graduate Group Chairperson

Daniel S. Kessler, Ph.D.

Associate Professor of Cell and Developmental Biology


Dissertation Committee

Wenqin Luo, M.D., Ph.D., Associate Professor of Neuroscience

Greg J. Bashaw, Ph.D., Professor of Neuroscience

Michael Granato, Ph.D., Professor of Cell and Developmental Biology

Minghong Ma, Ph.D., Professor of Neuroscience

**ACKNOWLEDGMENTS**

ABSTRACT

THE ROLE OF NEUROPILIN2A/B AND SEMA3FA IN THE PROTOGLOMERULAR

TARGETING OF ZEBRAFISH OLFACTORY SENSORY NEURONS

Ryan Pei-Yen Cheng

Jonathan A. Raper

During development, zebrafish olfactory sensory neurons (OSNs) project axons from the

olfactory epithelium to neuropil structures in the olfactory bulb (OB) known as

protoglomeruli. OSNs expressing either OMP or TRPC2 exclusively project axons to two

distinct, complementary sets of protoglomeruli. It is not known how differential

protoglomerular targeting of these two populations is maintained. The guidance

receptors *nrp2a* and *nrp2b,* along with their ligand *sema3fa*, were identified through

RNAseq as potential candidates responsible for differential protoglomerular targeting of

OMP- and TRPC2-class OSNs. *Nrp2a* and *nrp2b* are expressed in TRPC2-class OSNs,

while *sema3fa* is expressed in OMP-class OSNs and OB. To investigate the involvement

of these guidance factors in OSN axon guidance, the protoglomerular targeting fidelity of

OSNs expressing OMP:RFP or TRPC2:Venus were assessed in *nrp2a*, *nrp2b*, and

*sema3fa* mutants. The roles for these three guidance factors were further investigated

through genetic interaction studies and live time-lapse imaging experiments. Targeting

fidelity of TRPC2-class OSNs is degraded in *nrp2a*, *nrp2b*, and *sema3fa* mutants with

increased rates of misprojecting axons observed in OMP-specific protoglomeruli as well

as non-protoglomerular regions within the OB. Genetic interaction experiments suggest

that *nrp2a* and *nrp2b* are partially redundant and that *sema3fa* is likely one of multiple

guidance cues that acts in the same pathway as *nrp2a* and *nrp2b*. Live time-lapse

imaging experiments comparing *nrp2a* and *sema3fa* mutants to their heterozygous

siblings show that the dynamic behavior of TRPC2-class OSN growth cones are altered

in mutant animals. The results support a model in which *sema3fa* functions as a

repulsive cue to exclude *nrp2a-* and/or *nrp2b*-expressing TRPC2-class OSNs from

OMP-specific protoglomeruli as well as form the dorsal-medial OB, adding to a growing

list of guidance factors involved in protoglomerular targeting of OSNs. I also describe a

protocol for the registration of guidance cue expression data in the 36hpf OB and

present an unbiased registration template and model of the 72hpf OB and

protoglomeruli. This work highlights the complex interaction of guidance factors involved

in protoglomerular targeting of OSNs and lays a foundation for the systematic study of

olfactory circuit formation.

TABLE OF CONTENTS

LIST OF ILLUSTRATIONS

**CHAPTER 1: General Introduction**

Olfaction is likely one of the oldest means for organisms to sense the world around them. The basic structure of the vertebrate olfactory system has been conserved over 500 million years of evolution with specialized receptor molecules and organs for detecting both odorants and pheromones (Hoover, 2010). These same characteristics are shared with many invertebrates resulting from convergent evolution (Ha and Smith, 2009). The olfactory system allows organisms to detect odor molecules within the environment, encode this information into a neural representation, and interpret these signals to inform essential behaviors such as feeding, predator avoidance, and mate attraction in mouse (Boehm et al., 2005; Keller et al., 2009; Stowers et al., 2013), fish (Dieris et al., 2017; Hussain et al., 2013; Wakisaka et al., 2017; Yabuki et al., 2016), fly (Heimbeck et al., 2001; Ruta et al., 2010), and nematode (Bargmann and Horvitz, 1991; Edison, 2009; Macosko et al., 2009). The detection of odorants is accomplished by olfactory sensory neurons (OSNs) expressing odorant receptors (ORs) that selectively bind to different odor molecules. The detection of specific odors is transformed into a neural representation through the organization of the olfactory circuitry. This transformation entails the mapping of vast space of detectable odorants onto a topographic map in the brain. A recent estimate sets the number of detectable organic molecules based on physical properties at over 30 billion (Mayhew et al., 2021). The number of distinguishable olfactory percepts to which this corresponds is still unknown but likely not as high as the commonly cited number of over one trillion (Bushdid et al., 2014; Gerkin and Castro, 2015; Meister, 2015). Unlike the relatively straightforward mapping along spatial dimensions in the visual and tactile systems or along frequency in the auditory system, it is unclear over which physical or biological dimensions the odor map is organized. What is clear is that the precise and specific wiring together of the

olfactory neural circuits is essential for the proper function of the olfactory system. Conditional knockouts of the axonal guidance receptors Robo2 in OSNs or Nrp2 in mitral cells disrupt normal connectivity in different subsets of glomeruli and impair innate social behaviors in mice (Cho et al., 2011; Inokuchi et al., 2017). Elucidating the mechanisms that underlie the development of the glomerular map will further our understanding of the assembly of complex, stereotyped neural circuits. In this thesis, I examine the contribution that an important family of axon guidance receptors, the neuropilins, play in the formation of olfactory circuitry in the developing zebrafish. I also present new techniques I developed in this endeavor that will facilitate future studies of guidance factors involved in circuit formation in the olfactory system.

**Structure of the mouse olfactory system**

OSNs of the main olfactory system are located in the main olfactory epithelium on the roof of the nasal cavity as well as the Grüneberg ganglion and the septal organ. The olfactory epithelium (OE) consists of laminar folds that increase the surface area of the epithelium and is covered in a mucosal layer. This layer acts as the sensory interface where volatile odorants and the cilia of OSNs meet. The axons of OSNs project from the OE, along the olfactory nerve, and into the glomerular layer of the main olfactory bulb (MOB), where they synapse onto the dendrites of mitral and tufted cells. These projection neurons of the olfactory bulb (OB) in turn send projections to higher olfactory processing areas, including the anterior olfactory nucleus, taenia tecta, olfactory tubercle, piriform cortex, anterior and posterior amygdala, and the lateral entorhinal cortex (Reviewed in Suárez et al., 2012).

Vomeronasal sensory neurons (VSNs) in the vomeronasal system are found in the vomeronasal organ (VNO) located at the base of the nasal septum. The organ is a blind-

ended tube in which the microvilli of VSNs are exposed to external pheromones. VSNs

extend axons out of the VNO and into the accessory olfactory bulb (AOB) located dorsal-

posterior to the OB. VSNs synapse on to mitral cells in the AOB, which project to the

vomeronasal amygdala (Kang et al., 2011).

**Cellular components of the mouse olfactory system**

The most peripheral part of the vertebrate olfactory system is made up of OSNs. These

cells are the interface between the olfactory system and the chemical environment it

perceives. OSNs consist of hundreds or, in some species, thousands of subtypes. Each

subtype is defined molecularly by the exclusive expression of odorant receptors (ORs)

from a single allele (Malnic et al., 1999; Ngai et al., 1993; Ressler et al., 1993; Vassar et

al., 1993). OSNs expressing the same OR are stochastically distributed within large,

overlapping zones along the dorsal-ventral axis in the OE (Miyamichi et al., 2005;

Ressler et al., 1993; Vassar et al., 1993). The axons of OSNs expressing the same OR

converge on a pair of single glomeruli at stereotypical medial and lateral locations within

the OB (Ressler et al., 1994; Vassar et al., 1994; Zapiec and Mombaerts, 2015). The

zonal position of OSNs in the OE corresponds to the glomerular position in the olfactory

bulb along the dorsal-ventral axis (Zapiec and Mombaerts, 2020). This pattern of

stereotyped convergence converts a diffuse odorant experience into a stereotypical map

of neuronal activity in the bulb (Friedrich and Korsching, 1997, 1998; Wachowiak and

Cohen, 2001). At the end of development, OSNs expressing the same OR are

intermixed with OSNs expressing other ORs within the olfactory epithelium while their

axons all converge on one (zebrafish) or two (mouse) OR-specific glomeruli. The axons

that converge on each glomerulus form synapses with mitral and tufted projection

neurons which connect to the olfactory cortexes (Miyasaka et al., 2009; Stettler and

Axel, 2009). A topographic representation of odorant signals in the bulb is thus generated during development and is the basis of odorant discrimination in the vertebrate brain.

The mouse olfactory system is divided into two anatomically distinct structures, the main olfactory system (MOS) and the vomeronasal olfactory system (VNS), also known as the accessory olfactory system. The sensory neurons of the VNS, also known as VSNs, are located at the base of the nasal septum of the vomeronasal organ and each express one vomeronasal receptors (VRs) with one co-receptor (Dulac, 2000; Dulac and Axel, 1995; Halpern, 1987). The axons of these cells project through the cribriform plate, along the medial aspect of the OB, and to the AOB at the dorsocaudal end of the OB.

**Development of MOB Circuitry in the mouse**

Olfactory circuit formation has been extensively studied using the mouse model system. Beginning with the cloning of the ORs by Buck and Axel (1991), the field has come a long way in elucidating the mechanisms that underpin the coordination between OR expression and axon guidance. It has become clear that olfactory circuit formation in the mouse has both OR dependent and OR independent components. Both are required for formation of the stereotyped topographic glomerular map during development.

**Classical guidance factors in olfactory map formation**

It has been proposed that the OR independent component of OSN axon guidance organizes projections along the dorsal-ventral (DV) axis of the OB (Nishizumi and Sakano, 2015). It has long been known that a close correlation exists between the location of OSN cell bodies within the OE and the glomerular targets in the OB (Astic et al., 1987; Miyamichi et al., 2005). A correlation has also been observed between the

position of OSNs in the OE and the expression of a suite of axon guidance factors. Two sets of repulsive ligand/receptor pairs, Robo2/Slit1 and Sema3F/Nrp2, have been shown to have graded expression by OSNs in the OE.

Robo2 has been shown to be expressed in a gradient across the OE in a dorsomedial-high, ventral-low fashion, while Slit1 and Slit3 are expressed in the opposite gradient concentrated in the ventral OB (Cho et al., 2007, 2012). In Robo2 and Slit1 mutants, glomerular formation in the dorsal OB is disrupted, suggesting that repulsive Slit1 signals in the ventral OB help to organize Robo2-expressing OSNs to the dorsal OB (Cho et al., 2007, 2011, 2012). Robo2 is also required for the normal glomerular targeting of OSNs to the ventral parts of the OB (Cho et al., 2012). Slit1, Slit2, and Slit3 have all been shown to play a role in normal OSN axon guidance (Cho et al., 2007, 2012; Nguyen-Ba-Charvet et al., 2008). They are expressed both in the ventral OB and the axons of OSNs that project to the ventral OB, but it is unclear whether the effect of Slits on OSN axon guidance are mediated by expression at the target or along the way by neighboring axons (Cho et al., 2012).

The repulsive ligand Sema3F is also expressed in a gradient along the DV axis, high in the dorsal region and low in the ventral region, while its receptor Nrp2 is expressed along a gradient in the opposite direction (Norlin et al., 2001; Takeuchi et al., 2010). The expression levels of these guidance factors are also closely correlated with the OR subtype of each OSN. Loss of function of Sema3F or Nrp2 result in OSNs that project past the glomerular layer into deeper layers of the OB (Cloutier et al., 2004; Walz et al., 2002). Gain and loss of function experiments have shown that Nrp2 regulates axon projections along the DV axis (Takeuchi et al., 2010). During development, axons of OSNs in the dorsal OE project and arrive first at the olfactory bulb (Sullivan et al., 1995;

Takeuchi et al., 2010). These early axons express ROBO2 and SEMA3F. It has been proposed that SEMA3F secreted by dorsal OSNs repel ROBO2 expressing NRP2-expressing OSNs away from the dorsal OB (Takeuchi et al., 2010).

These observations support a model in which OSN axon guidance along the DV axis is regulated by the combined effects of Slit/Robo and Sema3F/Nrp2. Specifically, Robo2-expressing OSNs in the dorsal OE are the first to project the OB and restricted to the dorsal OB by Slit1. These early OSNs express Sema3F, which repels the late-arriving Nrp2-expressing OSN axons from the dorsal OB. This results in the organization and coordination of OSNs along the DV axis in the OE and the OB.

The current model of glomerular map formation is explained by axon guidance along the AP and DV axes, with Nrp1/Sema3A regulating the AP axis. Detailed study of the consequences of Nrp1 deletion in different populations and maturity levels of OSNs has challenged the AP component of the two-axis model (Assens et al., 2016; Zapiec et al., 2016). Assens et al., 2016 showed that the Nrp1 expression gradient among glomeruli is not smooth, with neighboring glomeruli often expressing vastly different amounts of Nrp1. This was also demonstrated through the quantification of Nrp1 expression in all glomeruli of a single OB (Zapiec et al., 2016). By disrupting Nrp1 signaling at different stages of OSN maturation, differing requirements for Nrp1 were uncovered. Early, but not late, deletion of Nrp1 recapitulated the anterior glomerular shift of MOR23-expressing OSNs described by Nakashima et al., 2013. Disruption of Nrp1 signaling in maturing OSNs resulted in dorsally shifted glomeruli for M71- and M72-expressing OSNs, while deletion of Nrp1 earlier in the process of OSN maturation resulted in the formation of both dorsally shifted glomeruli as well as ectopic glomeruli in the anterior OB. Taken together, these data suggest that OSNs have differential requirements for

6

Nrp1 signaling at different stages of maturation. When Nrp1 was deleted in M71-expressing OSNs in a mosaic fashion, wild type and ectopic glomeruli were both formed (Assens et al., 2016). Interestingly, $Nrp1^+$ and $Nrp1^-$ M71-expressing OSNs were observed to innervate both wild type and ectopic glomeruli. This suggests that once glomeruli are formed, Nrp1 signaling can be overridden by other guidance or adhesion mechanisms. The formation of anterior glomeruli when Nrp1 is deleted early is consistent with the current model. However, the dorsal shift of the M71 and M72 glomeruli suggest that the two-axis model may be insufficient to explain the coarse topographic organization of the glomerular map. It seems plausible that the shifts seen in these experiments are circumscribed by protoglomeruli and dependent on as yet unidentified axon guidance factors.

The OR dependent component of OSN axon guidance is thought to play a role both in the global targeting of axons in the OB as well as in finer scale axon coalescence during the formation of glomeruli. Both of these roles are mediated through cyclic adenosine monophosphate (cAMP)-dependent transcriptional regulation (Imai et al., 2006; Sakano, 2010).

In immature OSNs, spontaneous conformational changes of the OR between active and inactive states results in a variable but OR-specific baseline level of activity (Nakashima et al., 2013). This baseline activity is mediated through a G protein-coupled signaling pathway. Experimental manipulation of the baseline activity of an OSN using a highly active GPCR mutant resulted in a posterior shift of the resulting glomerulus, while lower activity mutants caused an anterior shift. OSNs expressing the highly active mutant receptors expressed increased levels of Nrp1, while OSNs expressing the lower activity mutant receptors expressed decreased levels of Nrp1 (Nakashima et al., 2013).

Increasing and decreasing Nrp1 expression in OSNs resulted in posterior or anterior glomerular shifts respectively (Imai et al., 2006). Beyond determining the positioning of glomeruli along the AP axis, Nrp1 also regulates the pre-target sorting of axons within the olfactory nerve. Along with Sema3A, Nrp1 contributes to the sorting of Nrp1-$^{high}$/Sema3A$^{low}$ axons to the outer-lateral compartment of the olfactory nerve and Nrp1-$^{low}$/Sema3A$^{high}$ axons to the central compartment (Imai et al., 2009). Together, these studies support a model in which OR-specific agonist-independent activity influences glomerular positioning by regulating the expression of axon guidance factors.

In mature OSNs, OR signaling is mediated though an olfactory-specific G protein ($G_{olf}$). $G_{olf}$ in turn activates adenylyl cyclase III, driving up cAMP levels, which opens cyclic-nucleotide gated (CNG) channels (Wong et al., 2000). The opening of CNG channels along with chloride channels results in the firing of action potentials (Stephan et al., 2009). The pattern of spontaneous neural activity of OSNs is dependent on the OR species (Nakashima et al., 2019). Evidence suggests that this spontaneous activity pattern is not inextricably linked to the odor response profile of the OR (Zhang et al., 2012). In other words, there does not appear to be a direct mechanism that maintains the one-to-one pairing between odor response of an OSN and its glomerular location. Nonetheless, optogenetic experiments suggest that these OR-specific neural activity patterns instruct the expression of axon-sorting guidance factors, specifically differential expression of Kirrel2, Sema7a, and PCDH10. This creates a combinatorial code of glomerular identity in the OB (Nakashima et al., 2019). The homophilic adhesion molecules Kirrel2 and Kirrel3 have been identified, along with EphA and its repulsive ligand ephrin-A, to be differentially expressed in different populations of OSNs (Serizawa et al., 2006). Kirrel2 and Kirrel3 were also shown to be required for normal glomerular

segregation in a subset of OSNs while dispensable for others (Vaddadi et al., 2019). Together, these studies suggest that OR-specific patterns of spontaneous neural activity control the expression of axon sorting factors, creating a combinatorial code which regulates the formation of OR specific glomeruli.

**Development of AOB circuitry**

VSNs project axons from the VNO to the AOB, where they form spatially conserved glomeruli (Wagner et al., 2006). VSNs with cell bodies in the apical layer of the VMO project to the anterior AOB, while VSNs in the basal layer project to the posterior AOB. Unlike the OSNs of the main olfactory system (MOS), VSNs expressing the same VRs innervate up to 30 different glomeruli in the AOB, but similar to the main olfactory system, each glomerulus is innervated only by VSNs expressing the same VR (Belluscio et al., 1999; Rodriguez et al., 1999). Many of the same guidance cues are implicated in the normal development of both the MOS and the VNS. Nrp2 is expressed by VSNs in the apical VNO (Cloutier et al., 2002). The Nrp2 ligand Sema3F is expressed by mitral cells in the AOB (Cloutier et al., 2002). Nrp2 and Sema3F mutants show defects in VSN axon guidance with axons misprojecting into the posterior AOB (Cloutier et al., 2002, 2004). Apical VSNs express high levels of Ephrin-A5. These axons are attracted by cells in the AOB that express EphA6 (Knöll et al., 2001). Robo2 is expressed by VSNs in the basal VNO and Slit1 is expressed in the anterior of the AOB (Cloutier et al., 2004; Knöll et al., 2003; Prince et al., 2009). Slit1, but not Slit2 or Slit3, is required for normal targeting of basal VSNs to the posterior AOB (Cloutier et al., 2004; Prince et al., 2009). Glomerular formation in the AOB is dependent on VR expression and regulated by postnatal sensory activity (Belluscio et al., 1999; Rodriguez et al., 1999). Similar to the mechanisms uncovered in the MOS, variable expression of kirrel2 and kirrel3 in different

subsets of VSNs is instructive in the normal segregation of axons into glomeruli. In Kirrel3 mutants, glomeruli loose VR exclusivity. Axons of VSNs expressing different VRs coalesce to form abnormally large glomeruli (Prince et al., 2013). Taken together, these observations suggest a model in which Nrp2/EphrinA5 expressing VSNs of the apical VNO project to the AOB and are restricted to the anterior AOB by repulsion from Sema3F expressed by mitral cells in the posterior AOB as well as attraction by EphA6. Basal Robo2 expressing VSNs are targeted to the posterior AOB by repulsive signals of slit1 at the anterior tip of the AOB. Once in the AOB, a VR-activity dependent mechanism either drives or cooperates with variable expression of Kirrel2 and Kirrel3 to regulate the sorting of axons in VR-specific glomeruli.

**Development of zebrafish olfactory circuitry**

There are 158 OR genes in the zebrafish genome compared to 1142 OR genes in mouse, making it a more manageable model for studying olfactory circuit development (Olender et al., 2020). Similar to mouse, each zebrafish OSN expresses from a single OR locus, with each OR being expressed in 0.5-2.5% of all OSNs (Barth et al., 1996, 1997; Sato et al., 2007). In larval zebrafish, OR expression does not appear to be patterned within the OE; however, in adults, OR expression is organized in overlapping concentric zones (Shao et al., 2017; Weth et al., 1996). OSNs are generated from the central and peripheral regions of the OE. Zonal expression of ORs in adult zebrafish results from biased expression of different subsets of OR subfamilies in these two zones coupled with the migration of OSNs during maturation (Bayramli et al., 2017). Mirroring what is seen in mammals, zebrafish OSNs expressing the same OR project to a single glomerulus in the mature bulb (Weiss et al., 2020). Zebrafish OSNs are born in the OE and send their projections along a scaffold of transient unipolar pioneer neurons

(Whitlock and Westerfield, 1998). The axons initially target large neuropil structures

known as protoglomeruli that are individually identifiable and reliably distinguishable at 3

days post-fertilization (dpf) (Dynes and Ngai, 1998). There are 11 identifiable

protoglomeruli at this stage (Lakhina et al., 2012). These neuropils are made up of the

axons of OSNs and the dendrites of neurons originating in the OB (Li et al., 2005).

The protoglomerular target of an OSN is tightly correlated to OR gene choice and

coordinated with the expression of axon guidance cues (Dang et al., 2018; Shao et al.,

2017). OSNs that express the same OR all project their axons to the same

protoglomerulus. Observations of protoglomerular targeting of samples of OR subfamily

members suggest that OSNs expressing ORs from the same subfamily all project axons

to the same protoglomerulus (Shao et al., 2017).

Reports suggest that protoglomeruli represent coarse functional domains as

demonstrated by stereotyped odor-evoked neural activity in the OB of larval zebrafish

(Koide et al., 2009; Li et al., 2005). Genetically encoded calcium indicators were used to

monitor odor-evoked responses in larval zebrafish. Exposing the larvae to different

classes of odors evoked different spatial response patterns in the OB (DeMaria et al.,

2013; Feng et al., 2005; Li et al., 2005). The observation of odor-specific neural

responses at early larval stages are consistent with the reports of odor-evoked behaviors

to biologically relevant odors as early as 4 dpf (Lindsay and Vogt, 2004). As

development continues, the axons within a protoglomerulus coalesce based upon OR

identity and form distinct glomeruli (Li et al., 2005). The formation of glomeruli occurs

both through experience-dependent and -independent pathways (Braubach et al., 2013).

By adulthood, the glomerular map is largely stereotyped, with some defined regions of

higher variability in both size and number of glomeruli (Braubach et al., 2013). It has

been proposed that this variability is an indication of the level of maturation of the individual glomeruli as a function of exposure to environmental stimuli (Braubach et al., 2013).

The zebrafish is a powerful model system for studying the development of the olfactory system. The accessibility of early larval stages of zebrafish has facilitated more detailed studies into the early stages of olfactory circuit formation as compared to mouse. Optogenetic manipulations, as well as fluorescence labeling, have been leveraged for investigations into the zebrafish olfactory system, including studies on the functional spatial maps in the OB, salt-sensing by OSNs, and odor-evoked behavior using optogenetic stimulation of OSNs (Bundschuh et al., 2012; Herrera et al., 2021; Jeong et al., 2021; Li et al., 2005). The system also has the potential for behavioral studies within the first week of development (Herrera et al., 2021; Jeong et al., 2021; Lindsay and Vogt, 2004). The feasibility of higher throughput experiments could translate to potentially greater sensitivity in assessing mutant phenotypes. The system is also amenable to detailed live imaging. This, in combination with the relatively fast development of the larval zebrafish olfactory system, allows for detailed observations of circuit formation in real time.

The development of olfactory circuitry is thought to occur in at least two steps. Global axon targeting generates a coarse protoglomerular map of OSN projections that is later refined into the final glomerular map. Studies in mice show that the location of OR-specific glomeruli may not be entirely invariable but are instead limited to a particular spatial domain within the bulb (Schaefer et al., 2001; Strotmann et al., 2000; Zapiec and Mombaerts, 2015). OR-dependent gene expression, driven by the OR specific spontaneous firing pattern (Nakashima et al., 2019), regulates adhesion molecule

expression on the axons of OSNs, driving sorting of OSNs into glomeruli (Serizawa et al., 2006). These observations are consistent with the notion of hierarchical axon guidance, where axon guidance processes first target OSN subtypes to specific protoglomeruli, after which a secondary sorting process further refines the projections into an OR-specific glomerular map. The zebrafish system is invaluable for the study of protoglomerulus formation, the first step in this process.

**Classical guidance factors in protoglomerular map formation**

Attractive signaling mediated by *Netrin/Dcc* plays a role in OSN protoglomerular targeting (Lakhina et al., 2012). *Dcc* is detected in a subset of OMP-class OSNs, including OSNs that express the transgenic *or111-7* reporter, which target the central zone (CZ) protoglomerulus. *Netrin1a* is expressed along the midline while *netrin1b* is expressed ventrally in close proximity to the site where the olfactory nerve enters the OB. Disruption of *Netrin/Dcc* signaling causes misprojections of OMP-class OSNs as well as OSNs expressing the *or111-7* reporter. Axon guidance of *or111-7*-expressing OSNs to the CZ is restored when Dcc is expressed in these cells in a Dcc knockdown background. The pattern of misprojections is consistent with a model in which *netrin1a* and *netrin1b* act as an attractive cue for a subset of OSNs expressing *Dcc*.

As in mouse, Slit/Robo signaling is important for OSNs axon guidance in zebrafish. Robo2 is expressed transiently in the developing olfactory placode between 20 and 36 hours post fertilization (hpf), while all four zebrafish slits (*slit1a*, *slit1b*, *slit2*, and *slit3*) are expressed in a distinct pattern surrounding the ventral-posterior and along the midline between the OEs (Miyasaka et al., 2005). In *robo2* mutants, the pioneer neurons often fail to enter the OB, misprojecting ventrally and posteriorly, and lead the later developing OSNs astray. A similar phenotype is observed when spatial pattern of repulsive cues is

13

disrupted by ubiquitous expression of *slit2* during axon outgrowth (Miyasaka et al., 2005). Protoglomerulus formation is also disrupted in *robo2* mutants; in particular, the three TRPC2-specific lateral protoglomeruli appear undifferentiated and form as a single protoglomerulus instead (Miyasaka et al., 2005; Sato et al., 2005).

In a more recent study, *robo2* was found to be preferentially expressed in a subset of OMP-class OSNs that target the dorsal zone (DZ) protoglomerulus (Dang et al., 2018). The protoglomerular target of an OSN is related to the OR clade from which it chooses to express an OR (Shao et al., 2017). Specifically, OSNs expressing ORs from clade A and B project to the CZ protoglomerulus, while OSNs expressing clade C ORs target the DZ protoglomerulus. Using single cell RNAseq, it was shown that the OSNs that express ORs from the same OR clade also express the same subset of axon guidance genes (Dang et al., 2018). In wild type animals, OSNs expressing a transgenic OR130-1 reporter (clade C) project to the DZ protoglomerulus. In *robo2* mutants, there is an increased number of OR130-1 reporter-expressing cells that misproject, particularly to the MG protoglomerulus (Dang et al., 2018). The projection pattern of OSNs expressing the *or111-7* reporter (clade A), which does not express *robo2*, was not affected in these mutants (Dang et al., 2018). These experiments show that Slit/Robo signaling is essential both for the early guidance of pioneer neurons and OSNs into the OB as well as for axon guidance within the OB. In the OB, *robo2* is likely required for the normal targeting of specific subsets of OSNs while dispensable for others.

Neuropilins and their ligands, the class 3 semaphorins, are also involved in protoglomerular map formation. This class of axon guidance cues have been shown to be required for OSN guidance in fly (Hong and Luo, 2014; Joo et al., 2013; Komiyama et al., 2007; Sweeney et al., 2011), mouse (Assens et al., 2016; Cloutier et al., 2002, 2004;

Imai et al., 2009; Inokuchi et al., 2017; Schwarting et al., 2000; Takeuchi et al., 2010; Taniguchi et al., 2003), and zebrafish (Dang et al., 2018; Taku et al., 2016). All four zebrafish neuropilins (*nrp1a*, *nrp1b*, *nrp2a*, and *nrp2b*) are differentially expressed in subsets of OSNs in the developing zebrafish olfactory system. Based on double *in situ* experiments, it has been shown that OSNs can express multiple neuropilins (Taku et al., 2016). Eight of the 12 zebrafish class 3 semaphorins are expressed in the developing olfactory system (Taku et al., 2016). At 36 hpf, *sema3aa*, *sema3ab*, *sema3fa*, *sema3ga*, and *sema3h* RNAs were detected in subsets of OSNs, while *sema3aa*, *sema3ab*, *sema3fa*, *sema3fb*, *sema3d*, *sema3e*, *sema3ga*, and *sema3h* RNAs were detected in the OB (Taku et al., 2016). In the OB, the detected *sema3*s have different overlapping patterns of expression (Taku et al., 2016). Many of the members of these two gene families come from the presumptive whole genome duplication event in teleosts, resulting in two orthologs for each of the two mouse neuropilins and two orthologs each for mouse Sema3A, Sema3F, and Sema3G (Glasauer and Neuhauss, 2014; He et al., 2019). Interestingly, despite the evolutionary divergence between mouse and fish for over 400 million years, the binding specificities of these neuropilin/semaphorin orthologs in the two systems remain very well-conserved (He et al., 2019). The distinct expression patterns of the zebrafish neuropilin and semaphorin paralogs suggest that they have gained specialized functions. It is still an open question as to how this specialization is used in the developing olfactory system.

The repulsive ligand *sema3d* is expressed in the anterior region of the developing zebrafish OB. In *sema3d* mutants, OSNs expressing the *or111-7* transgenic reporter misproject axons from the CZ to the DZ protoglomerulus (Taku et al., 2016). *or111-7* transgene-expressing OSNs express *nrp1a* and *nrp2b* and mutants for these genes

phenocopy *sema3d* mutants. Genetic interaction experiments between *nrp1a* and

*sema3d* suggest that *nrp1a* and *sema3d* cooperate to guide *or111-7* transgene-

expressing OSNs to the CZ protoglomerulus (Taku et al., 2016).

The *nrp1a/sema3d* phenotype is very similar to that seen *or111-7* transgene expressing

OSNs when *Netrin1b/Dcc* signaling is knocked down (Lakhina et al., 2012). The

expression pattern of *sema3d* is complementary to that of the attractive cue *netrin1b*,

and *nrp1a* and *dcc* are co-expressed in a large portion of *or111-7* transgene expressing

OSNs (Taku et al., 2016). Taken together, these results suggest that the attractive

*Netrin1b/Dcc* and repulsive *Nrp1a/Sema3d* signaling pathways cooperate to guide a

subset of OSNs to the CZ protoglomerulus.

*Nrp1a* is enriched in OSNs expressing 111 subfamily ORs (Clade A), while *nrp1b* is

preferentially co-expressed with 133 subfamily ORs (Clade C) (Dang et al., 2018). OSNs

expressing the *or111-7* transgenic reporter (Clade A) normally project to the CZ

protoglomerulus, but in *nrp1a* mutants, an increased rate of misprojections to the DZ

protoglomerulus is observed. OSNs expressing the *or130-1* transgenic reporter (Clade

C) normally project to the DZ but often misproject to the CZ in *nrp1b* mutants (Dang et

al., 2018). Based on these results, it is likely that *nrp1a* is important for axon guidance of

all Clade A OR-expressing OSNs, while *nrp1b* regulates protoglomerular targeting of

Clade C OR-expressing OSNs.

**OMP- and TRPC2-class OSNs**

There are no distinct anatomical structures that distinguish the main olfactory system

from the vomeronasal system in the zebrafish. However, the molecular components

corresponding to the two systems are found in distinct cell types within the zebrafish

olfactory system (Sato et al., 2005). The ciliated OSNs of the main olfactory system and the microvillous OSNs of the vomeronasal system are intermixed within the OE and can be distinguished by the differential expression of olfactory marker protein (OMP) or TRPC2 channels, respectively (Sato et al., 2005). Axons of the two populations of cells share a path from the OE to the OB but target mutually exclusive protoglomeruli in the OB (Sato et al., 2005). This organization is maintained throughout the lifetime of the animal. How the axons of these two populations segregate and differentially target their specific protoglomeruli in the bulb remains an open question.

**Differential targeting of OMP- and TRPC2-class OSNs is regulated by *nrp2a*, *nrp2b*, and *sema3fa***

In this thesis, I investigate the role of selected classical guidance molecules in the differential targeting of subsets of OSNs, specifically, how semaphorins and neuropilins regulate the deferential targeting of OMP- and TRPC2-class OSNs to their respective protoglomeruli. By analyzing protoglomerular targeting in different knockout conditions, I establish the requirement for *nrp2a*, *nrp2b*, and *sema3fa* in protoglomerular targeting of TRPC2-class OSNs. Genetic interaction experiments and live-imaging analysis suggest that these three guidance cues act in the same pathway to constrain the sample space of TRPC2-class OSNs. Additional cues, apart from *sema3fa*, likely act as ligands for *nrp2a* and *nrp2b* in this context.

To facilitate further investigations into additional guidance cues, I developed a protocol for registration and modeling of guidance cue expression within the olfactory bulb. The protocol uses a combination of custom scripts and commercial software for the reorientation and registration of 3D confocal datasets. Segmentation can then be performed to extract expression data. The protocol will facilitate the integration

expression maps generated from different experiments and allow for a better understanding of the guidance cue landscape of the developing olfactory system.

Our understanding of the development of the vertebrate olfactory system has greatly increased since ORs were first identified, but some outstanding questions remain. The organizing principles of OSN targeting are not yet resolved. It was proposed that global gradients of guidance factors along the rough AP and DV axes could explain early OSN targeting. This has been challenged by closer examinations of guidance cue expression data. Evidence in both mouse and fish are more consistent with an alternative model in which OSNs are targeted to defined regions of the OB, such as protoglomeruli in the fish. Another gap in our current understanding is how singular OR expression is coordinated with guidance factor expression. The OR expressed by an OSN has been shown to regulate the expression of certain guidance factors. On the other hand, OR swap experiments suggest that the general area an OSN targets within the bulb is not dependent on the OR it expresses (Wang et al., 1998). Lastly, the full compliment of guidance factors involved in OSN axon guidance has likely not yet been identified. Many guidance factors have been shown to be involved in OSN axon guidance, but their effects do not appear to be sufficient to fully explain OSN targeting patterns during development.

The experiments presented here add to a body of evidence that suggests that many guidance cues are expressed in overlapping but distinct patterns within the OB and cooperate to instruct axon targeting. Uncovering how the full complement of guidance cues works together to organize OSN axon guidance will be essential for understanding circuit formation in the developing olfactory system.

**CHAPTER 2: Loss of Neuropilin2a/b or Sema3fa Alters Olfactory Sensory Axon Dynamics and Protoglomerular Targeting**

Ryan P. Cheng, Puneet Dang, Alemji A. Taku, YoonJi Moon, Vi Pham, Xiaohe Sun, Ethan Zhao, Jonathan A. Raper

Author affiliations: Department of Neuroscience, University of Pennsylvania School of Medicine, Philadelphia, Pennsylvania 19104

Corresponding author: Jonathan A. Raper, raperj@mail.med.upenn.edu

**Abstract**

**Background:** Olfactory Sensory Neuron (OSN) axons project from the zebrafish olfactory epithelium to reproducible intermediate target locations in the olfactory bulb called protoglomeruli at early stages in development. Two classes of OSNs expressing either OMP or TRPC2 exclusively target distinct, complementary protoglomeruli. Using RNAseq, we identified axon guidance receptors *nrp2a* and *nrp2b*, and their ligand *sema3fa*, as potential guidance factors that are differentially expressed between these two classes of OSNs.

**Methods:** To investigate their role in OSN axon guidance, we assessed the protoglomerular targeting fidelity of OSNs labeled by OMP:RFP and TRPC2:Venus transgenes in *nrp2a*, *nrp2b*, or *sema3fa* mutants. We used double mutant and genetic interaction experiments to interrogate the relationship between the three genes. We used live time-lapse imaging to compare the dynamic behaviors of OSN growth cones during protoglomerular targeting in heterozygous and mutant larvae.

**Results:** The fidelity of protoglomerular targeting of TRPC2-class OSNs is degraded in *nrp2a*, *nrp2b*, or *sema3fa* mutants, as axons misproject into OMP-specific protoglomeruli and other ectopic locations in the bulb. These misprojections are further enhanced in *nrp2a;nrp2b* double mutants suggesting that *nrp2s* work at least partially in parallel in the same guidance process. Results from genetic interaction experiments are consistent with *sema3fa* acting in the same biological pathway as both *nrp2a* and *nrp2b*. Live time-lapse imaging was used to examine the dynamic behavior of TRPC2-class growth cones in *nrp2a* mutants compared to heterozygous siblings. Some TRPC2-class growth cones ectopically enter the dorsal-medial region of the bulb in both groups, but in fully mutant embryos, they are less likely to correct the error through retraction. The same result was

observed when TRPC2-class growth cone behavior was compared between *sema3fa* heterozygous and *sema3fa* mutant larvae.

**Conclusions:** Our results suggest that *nrp2a* and *nrp2b* expressed in TRPC2-class OSNs help prevent their mixing with axon projections in OMP-specific protoglomeruli, and further, that *sema3fa* helps to exclude TRPC2-class axons by repulsion from the dorsal-medial bulb.

**Introduction**

The precise wiring together of olfactory circuitry is essential for its proper function. Olfactory sensory neurons (OSNs) originate in the Olfactory Epithelium (OE) and send axon projections within the olfactory nerve to the Olfactory Bulb (OB). Each OSN expresses one or a few odorant receptor (OR) genes from a large gene repertoire (Malnic et al., 1999; Ngai et al., 1993; Ressler et al., 1993; Vassar et al., 1993). OSNs predominantly expressing the same OR are stochastically distributed within the OE while their axons converge on a single glomerulus at a stereotypical location within the OB (Ressler et al., 1994; Vassar et al., 1994). This pattern of stereotyped convergence converts a diffuse odorant experience into a stereotypical map of neuronal activity in the bulb (Friedrich and Korsching, 1997, 1998; Wachowiak and Cohen, 2001). In the zebrafish, OSNs first project axons to a set of distinct and identifiable intermediate neuropil targets in the olfactory bulb, known as protoglomeruli. Current information suggests that each protoglomerulus is the initial target for a subset of OSNs that all express closely related ORs (Shao et al., 2017). The axons in each protoglomerulus then further segregate to form distinct, OR-specific glomeruli (Dynes and Ngai, 1998; Li et al., 2005). In this report, we examine the contribution that an important family of axon guidance receptors, the neuropilins, play in protoglomerular targeting.

Neuropilins and their ligands, the semaphorins, function in olfactory axon targeting in flies, mice, and zebrafish (Fly: 13–16) (Mouse: 17–24) (Fish: 25,26) (see discussion for further details). A presumptive whole genome duplication event in teleosts has resulted in duplications of many members of these two gene families (Glasauer and Neuhauss, 2014). The zebrafish genome contains a pair of orthologs for each of the two mouse neuropilin genes, and one or two orthologs, twelve genes total, for each of the seven mouse class 3 semaphorins (He et al., 2019). Despite the nearly 400 million years of evolution separating the divergence of fish and mouse ancestral lines, the binding specificities of fish and mouse semaphorin/neuropilin orthologs are remarkably well conserved (He et al., 2019). Both semaphorin and neuropilin paralogs show distinct expression patterns within the developing zebrafish olfactory system, hinting at a division of labor for each paralog. How the developing nervous system exploits this specialization of paralog expression is an open question.

In tetrapod vertebrates, the main olfactory system and the vomeronasal system are divided, expressing different classes of odorant receptors (ORs as compared to V1R and V2R) and projecting to different areas of the olfactory bulb (the main and accessory olfactory bulbs) (Suárez et al., 2012). While the tetrapod main olfactory system is predominantly responsible for detecting classical odorants and the vomeronasal system is more specialized for pheromone detection, studies have shown that a subset of both classes of odorants are capable of activating both systems (Baum and Kelliher, 2009; Brennan and Zufall, 2006). In zebrafish, there are no anatomically distinct main olfactory and vomeronasal systems, though the molecular components of the two systems are separated and compartmentalized (Sato et al., 2005). Main olfactory system type ciliated OSNs and vomeronasal system type microvillous OSNs are mixed together within the

OE and can be distinguished by the ORs they express. OSNs expressing traditional ORs co-express Olfactory Marker Protein (OMP), while those expressing vomeronasal type receptors co-express TRPC2 channels. Both cell types extend axons within the olfactory nerve that segregate as they arrive at the OB–where they innervate mutually exclusive protoglomeruli (Sato et al., 2005). This segregation is maintained in the spatial distribution of OMP-class and TRPC2-class OSN axon glomeruli in the adult olfactory bulb (Sato et al., 2005). How these two populations of axons segregate apart from each other and differentially target specific protoglomeruli within the olfactory bulb is unknown.

We conducted an RNAseq-based screen to identify candidate signaling components that might be involved in the differential targeting of OMP as compared to TRPC2-expressing OSNs in the bulb (Shao et al., 2017). We compiled a list of candidate genes that are differentially expressed while between OMP and TRPC2 OSNs while their axons project to protoglomerular targets. The classical guidance receptors *nrp2a* and *nrp2b* were identified as candidates more highly expressed in TRPC2-class OSNs in this screen. We investigated the role that nrp2s play in protoglomerular targeting of TRPC2-expressing OSNs. Presumptive loss-of-function mutant lines demonstrate that each of these genes is required for accurate TRPC2-class OSN targeting. Through genetic interaction experiments, we show that *nrp2a* and *nrp2b* likely act in parallel to guide TRPC2-class axons to their targets. Further, we identify *sema3fa* as a likely ligand in the same signaling pathway as *nrp2a* and *nrp2b*. Using live imaging, we document TRPC2-class OSN axon guidance in high temporal detail and show that *nrp2a* and *sema3fa* are each required to exclude TRPC2-class OSN axons from the dorsal-medial region of the olfactory bulb.

## Methods

### Transgenic zebrafish lines

Adult zebrafish were raised and maintained according to standard procedures as previously described (Mullins et al., 1994). All experiments were conducted with the approval of the University of Pennsylvania Institutional Animal Care and Use Committee (IACUC). Veterinary care was supervised by University Laboratory Animal Resources (ULAR). Larvae were staged based on hours post fertilization (hpf) and were raised at 28.5°C. For some experiments, the 36 hpf time point was obtained by incubating for 1 day at 28.5°C and 1 day at 25°C (Kimmel et al., 1995). Tg(omp:lyn-RFP)rw035a and Tg(trpc2:gap-Venus)rw036a transgenic lines were obtained from the Yoshihara laboratory (Sato et al., 2005). Tg(omp:GAL4) and Tg(UAS:gap43-citrine) lines were described by Lakhina et al. (Lakhina et al., 2012).

### RNAseq of OMP and TRPC2 neuronal populations

RNAseq was performed as previously described (Shao et al., 2017). Single-cell suspensions of 48 hpf OEs were FAC sorted to obtained OMP:RFP-expressing and TRPC2:Venus-expressing cells. RNA was extracted and cDNA was synthesized using a custom oligo-dT primer. One round of *in vitro* RNA amplification was conducted for OMP-expressing neurons and two rounds for TRPC2-expressing neurons as previously described (Morris et al., 2011). Adapter-tagged libraries were synthesized using Illumina TruSeq v2.0 and deep-sequenced on a HiSeq2500 to obtain ~100 million reads per sample. Reads were mapped to *Danio rerio* genome assembly GRCz10 using the STAR algorithm (Dobin et al., 2013) and gene counts were generated using Verse (Zhu et al., 2016). Differential expression analysis was performed using DESeq2 (Love et al., 2014).

24

### *In situ* probe construction, hybridization, and fluorescent visualization

Single-label *in situ* hybridization was performed using antisense digoxigenin (DIG) RNA probes as previously described (Chalasani et al., 2007). *In situ* signals were amplified using a cyanine 3-coupled tyramide kit (TSA Plus Cyanine 3; PerkinElmer, NEL744001KT). Immunohistochemistry, propidium iodide labeling, and imaging were performed following tyramide amplification as described below in the immunohistochemistry section.

The plasmids used to make probes for *sema3fa* and *nrp2b* were gifts from the Moens laboratory at the Fred Hutchinson Cancer Research Center, Seattle, WA, USA (Yu and Moens, 2005; Yu et al., 2004). For *nrp2a* (refseq accession number NM_212965.1, nucleotides 138-1108) sequences were amplified from cDNA and cloned into pcRII (Invitrogen, K460001) for probe synthesis. Full-length probes were used in all hybridization experiments.

### Zebrafish Mutants

The *nrp2a*[p413] and *sema3fa*[p414] mutant alleles were generated by introducing a premature stop codon using CRISPR/Cas9 induced mutagenesis to insert a stop codon cassette as previously described (Gagnon et al., 2014) using Cas9 protein from PNA-Bio (CP01). Briefly, sgRNA sequences were identified using the CHOPCHOP web tool (Montague et al., 2014) (*nrp2a* target sequence, 5'-AGAGTGACCTCGGTTTGAGG-3') (*sema3fa* target sequence 5'- GAAGACTCGTGGAACAGAGG-3'). sgRNAs were generated using the pDR274 sgRNA expression vector as previously described (Hwang et al., 2013). pDR274 was provided by Keith Joung (Addgene plasmid # 42250). Corresponding stop codon cassettes were designed and synthesized for both target

sites and ordered as ssDNA oligos. Mutagenesis was performed by microinjection of the

sgRNA, stop codon cassette, and Cas9 protein into one cell-stage embryos. Stop codon

insertion was confirmed by standard PCR methods and sequencing. For *nrp2a*[p413], an

insertion was incorporated into exon 2, after base pair 116. The inserted sequence is (5'

- GTCATGCGTTTAAACCTTAATTAAGCTGTTGTAG - 3') and introduces a premature

stop codon and truncates the protein at position 191 of 927. For *sema3fa*[p414], an

insertion was incorporated into exon 2, after base pair 140. The inserted sequence is (5'

- GTCATGGCGTTTAAACCTTAATTAAGCTGTTGTAG - 3') and introduces a premature

stop codon and truncates the protein at position 43 of 801. Standard PCR-based

methods were used to genotype *nrp2a*[p413] (*nrp2a* forward primer, 5'-

CTCCGGGTTTCCCTGACAAG-3'; *nrp2a* reverse primer, 5'-

GACCTTCGACCTGGAGAACG-3') and *sema3fa*[p414] (*sema3fa* forward primer, 5'-

CCCATGCAGGACTGATAAATCTC-3'; *sema3fa* reverse primer, 5'-

CCACTGCTTTCCTGTTCAGATT-3'). The *nrp2b*[mn0126GT] mutants was a gift from the

Ekker laboratory at the Mayo Clinic, Rochester, MN, USA, and is available from ZIRC

(Clark et al., 2011). Standard PCR-based methods were used to genotype *nrp2b*[mn0126GT]

(*nrp2b* forward primer, 5'-GCTGAAGATCGGTATCAGACGAAAAACA-3'; *nrp2b* reverse

primer, 5'-AGACCTGCCATATTGGTGAGTACCGA-3'; RFP reverse primer, 5'-

CCTTGAAGCGCATGAACTCCTTGAT-3') lines. The *sema3fb*[sa14466] mutants were

acquired from the Sanger Center Zebrafish Mutation Project and obtained through ZIRC.

*sema3fb*[sa14466] is genotyped using a KASP assay (Biosearch Technologies) (KASP

sequence: 5'-

GAGTTCACAACCWTCACTGTGGATCAGGTCACAGCGGCCGACGGAAACTA[T/G]GA

GGTGCTSTTCCTGGGAACAGGTGAGTTTCATGATTTTTTTTTNNNCATGCA -3').

26

**Immunohistochemistry**

Immunohistochemistry was performed as previously described (Lakhina et al., 2012). Larvae were fixed in 4% paraformaldehyde in PBS and dehydrated in methanol. Larvae were permeabilized for 30 min in 0.1% collagenase at room temperature. To visualize Citrine-positive axons or Venus-positive axons, larvae were stained with goat anti-GFP (1:300; Rockland Immunochemicals, 600-101-215) and donkey anti-goat IgG Alexa Fluor 488 (1:500; Invitrogen). To visualize RFP-positive axons, larvae were stained with rabbit anti-dsRed (1:300; Clontech, 632496) and donkey anti-rabbit IgG Alexa Fluor 647 (1:500; Invitrogen). Propidium iodide staining was performed following secondary antibody treatment as described by (Brend and Holley, 2009), with the exception that larvae were not treated with RNase. Confocal microscopy was performed on an inverted Leica SP5 using a 63x oil-immersion lens. Z-stacks were acquired through the entire OB with optical sections taken 1µm apart.

**Quantification of targeting errors**

The number of OBs containing OMP- or TRPC- axons terminating in either individual protoglomeruli or non-protoglomerular regions were counted. Axons were scored as projecting to a particular protoglomerulus only if they terminated in that protoglomerulus and not if they passed though it en route to another location. The percentage of OBs with axon targeting errors was computed, and a two-tailed Fisher's exact test was used to determine statistical significance. The number of ectopic termination sites was computed, and a two-tailed Welch's unequal variance t-test was used to determine statistical significance. Two-tailed Fisher's exact test was used to determine statistical significance of misprojection patterns.

**Live Imaging and analysis**

32 hpf larvae were mounted as previously described (Godinho, 2011), except in a modified orientation. Briefly, larvae were anesthetized in E3 solution containing PTU and tricaine methanesulfonate until unresponsive and transferred to a 1% low-melting-point agarose (Sigma), E3 solution containing PTU and 80µg/mL tricaine at 37°C. Larvae were mounted on a chambered coverslip (µ-Slide 8 Well Glass Bottom - Ibidi #80827) with olfactory pits positioned downward facing against the cover glass and with bodies at around a 30° angle from the coverslip. Excess agarose was removed, and up to 6 total larvae were mounted in the same chamber. The chamber was filled with 1x PTU, 1x tricaine, E3 solution and covered to prevent evaporation. Live imaging was performed on a BioVision spinning-disk confocal microscope system consisting of a Leica DMi8 inverted widefield microscope, a Yokagawa W1 spinning-disk confocal microscope, and a Photometrics Prime 95B scientific complementary metal-oxide-semiconductor camera. Z-stack time series were acquired with VisiView software using a Plan-Apochomat 40x/1.3 Oil-immersion objective and 488 and 561 nm lasers for excitation. Larvae were kept at 28.5°C for the duration of the experiments in an environmental chamber surrounding the microscope. Z-stacks were imaged at 1µm sections at 10-minute intervals for up to 18 hours. Z-stacks were imported into FIJI for reorientation using the "TransformJ Rotate" function to set left and right OE level and olfactory nerve at 15° from vertical. Z-stacks of both hemispheres were cropped and left hemispheres were mirrored for analysis. Live imaging data was analyzed frame by frame to measure cumulative time in the dorsal-medial OB and maximum projection distance into the dorsal-medial OB. Two-tailed Welch's unequal variance t-test was used to determine statistical significance.

**Segmentation and 3D modeling**

*In situ* segmentation and modeling of *sema3fa* and *sema3fb* expression was performed

using Imaris 9.7 (Oxford Instruments). Z-stacks of six hemispheres for each gene were

manually aligned using OMP:gal4;UAS:Citirine expression for reference and the OB was

manually segmented to create a custom region of interest. *In situ* signals from all twelve

samples were segmented using the "Spot detection" function and aggregated.

Segmented objects were filtered for high correlation across samples.

3D modeling of live imaging datasets was performed using Imaris 9.7 for segmentation

and FIJI for preprocessing. Time-lapse z-stacks from multiple live imaging experiments

were aligned and registered in FIJI using the Fijiyama plugin (Fernandez and Moisy,

2021). Fluorescence intensity of the time-lapse z-stacks were normalized using the

"Bleach correction" option in the "Histogram matching" function in FIJI. Axon positions

were extracted by manual thresholding and converting to binary. Registered binary time-

lapse z-stacks were averaged to create time-lapse probability maps of axon positions.

Time-lapse probability maps were averaged along the time-axis to create probability

maps of axon positions for the live imaging experiment. The "Surface" function in Imaris

was used to segment the probability maps at defined intensities.

**Results**

**Expression patterns of *nrp2a*, *nrp2b*, and *sema3fa* in the developing zebrafish
olfactory system**

A striking feature of the zebrafish olfactory projection is that axons originating from OMP-

expressing OSNs and from TRPC2-expressing OSNs terminate in distinct and separate

protoglomerular neuropils in the OB (Fig. 1A, Additional file 1). The guidance

mechanisms controlling this differential targeting are unknown. We reasoned that axonal

guidance receptors that are differentially expressed in OMP-class as compared to

TRPC2-class OSNs are candidates for mediating this differential targeting. We used an

RNAseq-based approach to identify candidate axonal guidance receptors expressed at

different levels in these two classes of OSNs. Main olfactory OMP-class OSNs and

'vomeronasal' TRPC2-class OSNs were separated and collected by FAC sorting from

dissociated cell suspensions prepared from the heads of transgenic OMP:RFP;

TRPC2:Venus 48 hpf embryos. At this developmental stage, axons of both classes of

OSNs are actively extending into the olfactory bulb. Bulk RNAseq was performed

separately on OMP-class and TRPC2-class OSNs in quadruplicate (Shao et al., 2017),

and differentially expressed genes were identified by DESeq2 (Love et al., 2014). The

canonical guidance receptors *nrp2a* and *nrp2b* were found to be expressed at a higher

level in TRPC2-class as compared to OMP-class OSNs (Fig. 1B). *In situ* probes for

*nrp2a* and *nrp2b* mRNAs confirm their enhanced expression in TRPC2-class OSNs at

48hpf(Fig. 1C-E). We found that *nrp2a* and *nrp2b* RNAs are detected in overlapping

subsets of TRPC2-class OSNs (Fig. 1D).

To identify potential neuropilin ligands that might serve as TRPC2-class axonal guidance

cues, we first examined class III semaphorins that preferentially bind *nrp2s*. A variety of

class III semaphorins can bind and signal through holoreceptors composed of Nrp2 and

PlexinAs (Sharma et al., 2012). Previous binding studies *in vitro* showed that Sema3fa,

Sema3fb, Sema3ga, and Sema3gb all preferentially bind to either Nrp2a or Nrp2b as

compared to Nrp1a or Nrp1b (He et al., 2019). We probed the developing olfactory

system for a variety of class III semaphorins by *in situ* hybridization of whole mount

heads (data not shown). One of these candidate ligands, *sema3fa*, was expressed in OMP-class OSNs (Fig. 1F). *Sema3fa* mRNA was detected on average at a higher level in OMP-class as compared to TRPC2-class OSNs by RNAseq, although there was too much variance between replicates for the difference to be considered significant (Fig. 1B). *Sema3fa* mRNA is also detected in the anterior and dorsal-medial regions of the 48 hpf OB (Fig. 1G).

**Nrp2a, nrp2b are required for normal protoglomerular targeting of TRPC-class OSNs**

To test whether *nrp2a* or *nrp2b* are required for normal protoglomerular targeting, we generated a mutant allele for *nrp2a* by CRISPR/Cas9 knock in of a multi-reading frame stop codon cassette (Gagnon et al., 2014) and took advantage of an existing gene-trap mutant allele for *nrp2b* (Clark et al., 2011). Each of these alleles are likely nulls since they introduce premature stop codons into early exons that cannot be skipped without shifting the frame of translation. These mutants were crossed into fish incorporating OMP:RFP and TRPC:Venus transgenic reporters to generate *nrp2a+/-*;OMP:RFP; TRPC:Venus or *nrp2b+/-*; OMP:RFP; TRPC:Venus lines. These lines were then crossed to themselves to determine how the loss of either *nrp2a* or *nrp2b* would affect protoglomerular targeting. Embryos were collected at 3 days post fertilization (dpf), genotyped, and processed for imaging. Confocal optical slices through the entire olfactory bulb were used to reconstruct OMP-class and TRPC2-class OSN axon trajectories. Counter staining with propidium iodide labeled nuclear material in all cell bodies and its absence allows the visualization of individual protoglomeruli neuropils. The fidelity of protoglomerular targeting was assessed by scoring for the presence of OMP-class or TRPC2-class OSN axon termini in each individual protoglomerulus.

31

Termini present in non-protoglomerular regions of the OB were also noted. Scoring was performed independently by two individuals blind to the genotypes of the embryos.

*Nrp2a* mutant animals had a higher rate of misprojecting TRPC2-class OSN axons as compared to wild type siblings (Fig. 2A,B). TRPC2-class axons misprojected to an average of 0.476 ectopic locations per OB hemisphere, a statistically significant increase relative to the 0.167 error rate in wild type siblings. These misprojections tended to concentrate in the MG protoglomerulus, anteriorly, and other non-protoglomerular regions (Fig. S1A). *Nrp2b* mutant animals also had a statistically higher rate of misprojecting TRPC2 expressing OSNs as compared to wild type siblings (Fig. 2C,D). TRPC2-class axons projected to an average of 0.533 ectopic locations per OB hemisphere as compared to a 0.294 error rate in their wild type siblings. These misprojections were concentrated in the LG3 protoglomerulus (Fig. S1B).

### *Nrp2a and nrp2b* act in a partially redundant, parallel signaling pathway

*Nrp2a* and *nrp2b* are paralogs that are orthologous to mammalian *nrp2*. The two genes have overlapping expression within the TRPC2-class of OSNs. Since the phenotype for neither mutant allele was fully penetrant, it is possible that *nrp2a* and *nrp2b* serve partially redundant functions in regulating protoglomerular targeting of TRPC2-class OSNs. To further test this idea, we generated *nrp2a+/-;nrp2b+/-* fish containing the OMP:RFP and TRPC2:Venus transgenic reporters. These fish were crossed together to generate siblings of all genotypes ranging from wild type to *nrp2a;nrp2b* double mutants. The fidelity of protoglomerular targeting was not significantly different in *nrp2a+/-;nrp2b+/-* trans-heterozygotes as compared to wild type siblings (not shown). The *nrp2a-/-* and the *nrp2b-/-* single mutant animals replicated the misprojection phenotypes

observed in the previous single mutant experiments (Fig. 3A,B). *nrp2a-/-;nrp2b-/-* double mutant animals had a statistically significant enhancement of the TRPC2-class OSN misprojection phenotype as compared to either single mutant alone, and this phenotype was nearly fully penetrant (Fig. 3A,B).

Quantifying the percentage of OB hemispheres with misprojections is a sensitive measure of infrequent misprojections at a population level; however, this measurement becomes saturated when used on highly penetrant phenotypes. To better represent the more robust misprojection phenotype in the nrp2a-/-;nrp2b-/- double mutants, we counted the number of inappropriate protoglomerular and non-protoglomerular targets (ectopic termination sites) occupied by TRPC2-class OSNs in each sample. TRPC2-class OSNs in double mutants projected to a significantly higher number of ectopic termination sites as compared to their single mutant or wild type siblings. Since targeting errors in single mutant or wild type embryos are nearly always comprised of single axons, while multiple overlapping axons sometimes contribute to the errors in double mutant embryos, our scoring underrepresents the number of misprojecting axons in the double mutant samples. Despite this relative undercounting, TRPC2-class axon misprojections were greater in double mutants (3.38 inappropriate protoglomerular targets per OB hemisphere) than in *nrp2a* and *nrp2b* single mutants combined (1 and 1.3 = 2.3 inappropriate protoglomerular targets per OB hemisphere). Significantly higher rates of misprojections to the OMP-class CZ, DZ, LG3, and MG target protoglomeruli were observed in double mutants as compared to the two single mutants combined (Fig. S1D). This error enhancement in the double mutants may be more than purely additive, suggesting that *nrp2a* and *nrp2b* act in a partially redundant, parallel signaling pathway to regulate protoglomerular targeting of TRPC2-class OSN axons.

Next, we asked whether the misprojection phenotype in *nrp2* mutant embryos represents a lasting alteration to olfactory circuitry or if targeting errors are corrected as development progresses. Wild type and *nrp2a;nrp2b* double mutant sibling 3 and 6 dpf embryos were compared. There was a small but statistically significant increase in the extent of misprojections observed at 6 dpf as compared to 3 dpf in double mutants (Fig.3C,D). This small increase in error rate might be explained by increasing numbers of TRPC2-class OSN axons innervating the bulb at the later developmental age. Nevertheless, these observations suggest that TRPC2-class OSN misprojections are not corrected during larval development.

**Sema3fa is required for normal TRPC2-class OSN protoglomerular targeting**

*Sema3fa* is a member of the Class 3 semaphorin family and has been shown to bind with Nrp2a and with Nrp2b in preference to Nrp1a or Nrp1b (He et al., 2019). It is expressed in OMP-class OSNs (Fig. 1F) and *in situ* probes for *sema3fa* mRNA detected its expression in the anterior OB in a region that extends into the dorsal-medial OB at 36hpf (Fig. 1G). To test whether *sema3fa* is required for normal protoglomerular targeting, we used CRISPR/Cas9 to generate a *sema3fa* mutant allele following the protocol described in Gagnon et al 2014 (Gagnon et al., 2014). The resulting allele is likely a null because the inserted stop codon cassette introduces an in-frame premature stop codon in an early exon that cannot be skipped without putting the translation product out of frame. It was crossed into fish containing OMP:RFP; TRPC2:Venus and the progeny of crosses between these fish were assessed for protoglomerular targeting fidelity as previously described. TRPC2-class OSNs in *sema3fa-/-* animals had an increased rate of misprojections compared to wild type siblings. TRPC2-class OSNs misprojected to 0.67 incorrect targets per OB hemisphere in *sema3fa* mutants as

34

compared to 0.13 incorrect targets in wild type siblings. The misprojections mostly consisted of targeting errors into CZ and LG3 protoglomuli.

While *sema3fa* mutants show increased rates of misprojections of TRPC2-class OSNs (1 inappropriate protoglomerular targets per OB hemisphere), the misprojection phenotype does not fully account for the much more severe *nrp2a-/-;nrp2b-/-* phenotype (3.38 inappropriate protoglomerular targets per OB hemisphere). This suggests that other Nrp2 ligands are involved in *nrp2*-dependent OSN axon guidance. One possible candidate is the Nrp2a- and Nrp2b-specific binding partner, Sema3fb, which we identified based on its expression in the OB. Sema3fb mRNA was detected in the dorsal OB with particularly high levels in the dorsal-medial area of the OB at 36hpf. This expression pattern fit with the potential function of Sema3fb as a repellent cue for Nrp2a- or Nrp2b-expressing OSNs. A likely null *sema3fb* mutant line (sa14466) was acquired, carrying a nonsense mutation that results in a premature stop codon. No increase in TRPC2- or OMP-class OSN axon misprojections were detected in *sema3fb* mutants (Fig. 4C). We also found no increase in the rate of TRPC2- or OMP-class OSN axon misprojections in *sema3fa-/-;sema3fb-/-* as compared to *sema3fa-/-* siblings (Fig 4C). We conclude that *sema3fb* cannot account for the additional errors in *nrp2a;nrp2b* double as compared to *sema3fa* mutant embryos, and that additional unknown Nrp2 ligands remain to be identified.

**Both *nrp2a* and *nrp2b* act in the same pathway with *sema3fa***

The similar mutant phenotypes in *nrp2a*, *nrp2b*, and *sema3fa* mutants suggest that they may act in the same signaling pathway to regulate TRPC2-class OSN protoglomerular targeting. One prediction from this hypothesis is that if *nrp2a* and *sema3fa* act in the

same pathway, the double mutant phenotype should be less severe than the effects of the two single mutant phenotypes added together. To test if this is true, we generated *nrp2a+/-;sema3fa+/-*; OMP:RFP;TRPC:Venus fish. These animals were crossed to generate wild type, single mutant, and double mutant siblings for comparison. *Nrp2a* and *sema3fa* mutants from this cross had the expected TRPC2-class OSN misprojection phenotype observed previously, and *sema3fa* mutant animals had a slightly stronger misprojection phenotype as compared to *nrp2a* mutant animals. The phenotype of *nrp2a-/-;sema3fa-/-* fish was not significantly different from that of the *sema3fa-/-* mutant. Neither the number of misprojections nor the pattern of misprojections were significantly different between *sema3fa-/-* and *nrp2a-/-;sema3fa-/-* animals. Similarly, the number of misprojections and the pattern of misprojections were not significantly different between *sema3fa-/-* and *nrp2b-/-;sema3fa-/-* animals. These results are consistent with Sema3fa acting as a ligand for both Nrp2a and Nrp2b in guiding TRPC2-class OSN axons to their protoglomerular targets.

**Misprojecting growth cones fail to retract in *nrp2a* and in *sema3fa* mutants**

One advantage of the zebrafish model system is the ability to examine the dynamics of developmental processes with live imaging. We took advantage of this to compare the development of OMP- and TRPC2-class projections in mutant larvae to heterozygote siblings. OMP:RFP; TRPC2:Venus embryos were mounted in agarose and imaged live between 30 hpf and 48 hpf. Spinning disk microscopy generated a z-stack through each olfactory projection every 10 minutes during this 18-hour period. This allowed us to visualize individual TRPC2-class axons and follow them as they projected into the olfactory bulb.

OMP:RFP and TRPC2:Venus expressing OSN axons have entered the OB at 30 hpf. OMP-class axons form a relatively compact bundle within the bulb. TRPC2-class axons occupy lateral and ventral-medial areas surrounding OMP axons. OMP- and TRPC2-class axons do not intermix freely. The relative organization of OMP and TRPC2 axons at this early stage is similar to that at 3 dpf, with the notable difference that protoglomeruli have not yet formed. As development continues, OMP-class axons separate into distinct clusters that become recognizable as the CZ, DZ, MG, and LG3 protoglomeruli at around 36 hpf. More TRPC2-class axons arrive in the OB and begin to form recognizable protoglomeruli by 38 hpf. Throughout this time period, TRPC2-class axons in particular can be seen dynamically extending and retracting in the OB, probing and retreating from areas larger than their ultimate protoglomerular targets.

To investigate whether the behavior of TRPC2-expressing OSN axons are affected in *nrp2a* mutants, *nrp2a*-/- animals were crossed to *nrp2a*+/- animals carrying OMP:RFP; TRPC2:Venus. The resulting embryos were live-imaged and subsequently genotyped after imaging. Just as in wild type fish, TRPC2-class axons are confined to ventral and ventral-lateral regions of the OB in *nrp2a*+/- embryos (Additional file 3). In *nrp2a*-/- embryos, we observed TRPC2-class axons entering into, and remaining within, the dorsal-medial region of the OB that is normally not occupied by TRPC2-class axons (Additional file 4). To quantify this phenotype, we defined the dorsal-medial OB as the region of the bulb dorsal to CZ and DZ protoglomeruli (Fig. 6, yellow dotted lines). In *nrp2a* mutant embryos, the time that TRPC2-class axons occupy the dorsal-medial OB is greater than in their *nrp2a*+/- siblings (386 vs 95.35 minutes; Fig. 6A,B). Axons also extend farther in *nrp2a*-/- as compared to heterozygous siblings, extending on average 10.65 µm past the CZ-D boundary compared to 7.47 µm (Fig. 6A,C).

The same experimental protocol was used to study *sema3fa* mutants. We observed an increased occupancy time in the dorsal-medial OB by TRPC2-class axons in *sema3fa* mutants as compared to heterozygous siblings (Additional file 5 and 6). The dorsal-medial OB was occupied on average 426.5 minutes in mutant animals as compared to 58.44 minutes in heterozygous siblings (Fig. 6D,E). The distance that misprojecting TRPC2-class axons extended past the CZ-DZ boundary was also greater in *sema3fa* mutants as compared to heterozygotes (Fig. 6D,F).

To get a better sense of the overall behavior of TRPC2-class axons in *sema3fa* heterozygotes vs mutants, we generated a 3D model of the live imaging dataset from six samples of each genotype (Fig. 6G). To create a probability map of axon locations, z-stacks of all 12 samples were aligned in 3D space. Each z-stack was converted to binary to normalize fluorescence intensity, and the resulting 3D time series were summed together to create an averaged time series. The time series was further summed along the time axis to create a 3D probability map of axon locations. Consistent with the manual quantification, comparing the 3D models for *sema3fa* heterozygotes to *sema3fa* mutants shows an increased probability of finding TRPC2 axons in the dorsal-medial OB (Fig. 6G).

We occasionally observed apoptosis of individual OSNs and the subsequent fragmentation of their corresponding axons (Additional file 4 and 5). Cell death was unlikely to have been induced by phototoxicity or other experimental procedures, since it was not increased by high laser illumination that caused widespread photobleaching of the fluorescent OSNs. Apoptosis was not observed more frequently in either *sema3fa* or *nrp2a* mutants as compared to heterozygote siblings, suggesting that cell targeting errors may not be corrected through cell death at this stage of olfactory circuit formation.

38

Our results indicate that *nrp2a* and *sema3fa* are required early in the development of olfactory circuitry to exclude TRPC2-class axons from specific regions of the olfactory bulb and that these errors are not quickly corrected.

**Discussion**

This study began with the observation that the RNAs for the axonal guidance receptors *nrp2a* and *nrp2b* are more highly expressed in TRPC2-expressing OSNs than in OMP-expressing OSNs, while *sema3fa* mRNA is well expressed in OMP expressing OSNs. As Sema3f is a known ligand for Nrp2 (Chen et al., 1997) and in most instances mediates repellent activity (Chen et al., 1998; Sharma et al., 2012), we hypothesized that the differential expression of these two signaling components may participate in the differential targeting of OMP- and TRPC2-class OSN axons to mutually exclusive protoglomeruli in the olfactory bulb. One mechanism through which this could occur is Sema3fs secreted by OMP-class processes repel TRPC2-class axons as they project towards and within the olfactory bulb. The two classes of axons are intermixed within the OE, but they separate as they enter the bulb. Fascicles of TRPC2-class axons surround a dense cable of OMP-class axons, like vines growing on the trunk of a tree. These separate TRPC2-class axon fascicles then terminate in ventromedial (OP) and dorsolateral (LG1, LG2, LG4, VPG) protoglomeruli that surround a cluster of OMP-class protoglomeruli (CZ, DZ, MG, LG3). If Sema3fa secreted from OMP-class axons helps to separate the two classes of axons, loss of *sema3fa* would be expected to induce ectopic fasciculation of TRPC2-class axons into OMP-class fascicles; no such mixing was detected. If another class 3 semaphorin functionally substitutes for *sema3fa*, mixing might be induced by the loss of *nrp2a*, *nrp2b*, or both; again, no such mixing was detected. These findings suggest that neither Sema3fa-nor Nrp2a/b-mediated signaling

39

play a decisive role in the selective fasciculation of OMP- and TRPC2-class axons.

We find, however, that the exclusivity in protoglomerular targeting of OMP- and TRPC2-class axons to distinct and complementary protoglomeruli is degraded in the absence of Nrp2a, Nrp2b, or their repellant ligand Sema3fa. In these mutants TRPC2-class axons invade protoglomeruli that are normally exclusively occupied by OMP-class axons. Sema3fa produced by OMP-class OSNs and released from their processes may help to repel, and thereby exclude, Sema3fa-sensitive TRPC2-class axons from OMP-class protoglomeruli. This parallels findings in mice: VNO axons in the mouse, the class most similar to TRPC2-class OSNs in fish, occasionally peel off VNO axon fascicles and enter into and form glomeruli in ectopic Main Olfactory bulb territories in both *Sema3F* or *Nrp2* mutants (Cloutier et al., 2002, 2004). It has been hypothesized that in mouse, secreted semaphorins surrounding the vomeronasal nerve help promote its fasciculation in a Nrp2-dependent manner (Cloutier et al., 2004). As we are proposing for the fish, Sema3F is thought to be secreted from Main Olfactory OSN axons in mice that are analogous to the OMP-class axons in fish (Inokuchi et al., 2017). Sema3fa/Nrp2 mediated repulsion cannot be the only mechanism that keeps OMP- and TRPC2-class axons from entering each other's protoglomeruli in the fish, as there is limited mixing of the two classes of axons in either *sema3fa* mutants or in *nrp2a*;*nrp2b* double mutants.

A second striking axonal misguidance phenotype in *nrp2a*, *nrp2b*, or *sema3fa* mutants is an increase in TRPC2-class axons extending ectopically into the dorsal-medial region of the olfactory bulb. Both end-stage analysis and time-lapse studies show a higher probability of TRPC2-class axons occupying this region of the bulb in mutant embryos. One interpretation of this phenotype is that the expression of Nrp2 guidance receptors is required for TRPC2-class axons to detect repellent semaphorins expressed in the

40

dorsal-medial OB. One of these repellents appears to be Sema3fa, since the same guidance phenotype is observed in *sema3fa* mutants. Sema3fa mRNA is detected along the anterior and dorsal-medial regions of the developing OB. *In situ* localization of other Nrp2 binding Sema3s (*sema3e*, *sema3fa*, *sema3fb*, *sema3ga*, *sema3h*) indicate that sema3e and sema3fb are also expressed in the dorsal-medial OB. We obtained a presumptive null *sema3fb* mutant line (Sanger sa14466) but did not observe increased ectopic TRPC-class axon entry into the dorsal-medial OB in these mutant fish. We have not examined *sema3e* mutant fish.

*Nrp2* has been shown to be required for normal axon guidance of subsets of MOB type OSNs in both the mouse and fish (Takeuchi et al., 2010; Taku et al., 2016). Nrp2-expressing OSNs may be restricted to the ventral-posterior region of the mouse MOB by responding to OSN-secreted Sema3F in the dorsal and anterior OB (Inokuchi et al., 2017; Takeuchi et al., 2010). OSN-secreted Sema3F also acts as a repellant cue for Nrp2-expressing mitral cells, olfactory projection neurons in the bulb (Inokuchi et al., 2017). In a previous study in the fish, loss of *nrp2b* induced misprojections of *or111-7* expressing OSN axons from their normal target, the Central Zone protoglomerulus, to the Dorsal Zone protoglomerulus (Taku et al., 2016). As all OMP-class axons were uniformly labeled in the experiments in this study, we were not able to detect mistargeting of OSN subpopulations within specific OMP-class protoglomeruli. However, ectopic extension of OMP-class axons outside their normal protoglomeruli should be visible, and we did not detect any such events in *nrp2a*, *nrp2b*, or *nrp2a*;*nrp2b* double mutant embryos.

The zebrafish system is nearly ideal for following the early stages of olfactory circuit development in live preparations. In pioneering live imaging studies, Dynes and Ngai

41

(Dynes and Ngai, 1998) visualized sparsely labeled fluorescent OSN axons at 1-hour

intervals. They concluded from their observations that OSN axons grow directly to their

targets without stopping at intermediate targets and without sampling inappropriate

target areas. With the more advanced microscopic techniques now available, we were

able visualize a larger number of growing OSN axons in three dimensions at more

frequent 10-minute intervals, and as a consequence were able to visualize the dynamic

searching behavior of individual sensory axon growth cones. We observed the basal to

apical migration of OSNs as they mature within the OE. We also noted the occasional

apoptosis of OSNs along with the fracturing and degeneration of their axons as descried

in previous studies (Dynes and Ngai, 1998). Most importantly, we observed that

individual OSN axons explore a larger area within the olfactory bulb outside their final

target location. We observed individual TRPC2-class axons extending and retracting

multiple times, sometimes extending the entire length of the OB and retracting back to

more proximal locations within an hour. TRPC2-class axons can therefore sample large

areas before settling on a defined target. In either *nrp2a* or *sema3fa* mutants, TRPC2-

class axons extended within and occupied the dorsal-medial OB for greater periods of

time than in heterozygous animals. In the heterozygotes, the axons that extend into this

region quickly retract proximally, while in mutant animals, TRPC2-class axons explore

this space for longer periods. Lack of either *nrp2a* or *sema3fa* appears to prolong the

duration of TRPC2-class occupation of the dorsal-medial OB, likely through the removal

of a repellent signaling pathway that would normally chase them from the region. This

live imaging approach increases the sensitivity of our mutant phenotype analysis. It also

suggests that altered axon dynamics could be a useful marker for future investigation of

OSN axon guidance factors.

A small number of TRPC2-class OSNs have misprojecting axons in either *nrp2a* or *nrp2b* mutants. These axons erroneously project into OMP-specific protoglomeruli or misproject dorsally into non-protoglomerular regions of the OB. This misprojection phenotype is much more severe and is fully penetrant in *nrp2a;nrp2b* double mutant animals. Our results imply that *nrp2a* and *nrp2b* receptors play partially redundant but largely parallel roles in the same guidance process. We cannot be certain that the sensitivity of *nrp2* mRNAs by *in situ* detection provides a truly reliable picture of physiologically relevant levels of *nrp2* expression. It is therefore possible that both *nrp2s* are expressed in most or all TRPC2 class neurons. It is formally possible that the two *nrp2s* work best together in a heterodimeric complex and less efficiently in homodimeric complexes, accounting for the partial redundancy of function between the two. More likely, however, is that each *nrp2* contributes to the pathfinding abilities of a distinct but overlapping population of OSNs. The non-overlapping subset of each population may be selectively affected by the loss of one or the other *nrp2*, while all cells in the two populations would be affected by the loss of both *nrp2a* and *nrp2b*. This interpretation is consistent with our detection of *nrp2a* and *nrp2b* mRNAs in overlapping subsets of OSNs.

The early teleost genome is posited to have undergone a duplication event subsequent to its divergence from terrestrial vertebrates (Glasauer and Neuhauss, 2014). As a consequence, zebrafish possess two paralogs of *nrp2* and several of the class 3 semaphorins. Many paralogous genes are expressed in divergent expression patterns in the embryonic fish. As a rule, each semaphorin paralog has a conserved neuropilin binding profile as compared to either its paralog or its corresponding mouse ortholog (He et al., 2019). It is unclear to what degree each paralog is specialized in its developmental

function. In this study, we find that the two *nrp2* paralogs have similar guidance functions for a distinct subset (TRPC2-class) of sensory neurons. Interestingly, this is not the case for the two *sema3f* paralogs. This suggests that in practice paralogs, can either work semi-redundantly, as the do the nrp2s, or a more specialized and independent fashion, as do the sema3fs.

Partial functional redundancy, as for example between *nrp2a* and *nrp2b*, between axonal guidance receptors expressed in overlapping populations of neurons would be expected to provide some level of robustness in neuronal circuit formation. A nearly identical principal has been elegantly expounded for the determination of neuronal identity (Hong and Luo, 2014). In both cases, no single gene would be decisive, as outcomes would depend on the effects of several genes with similar functions. In our experience, loss of any single guidance cue or receptor has thus far produced relatively low frequencies of targeting errors in the developing zebrafish olfactory system, while as expected, error frequencies increase when two guidance-related genes are knocked out together. As this study and others (Dang et al., 2018; Taku et al., 2016) have shown, loss of *nrp1a*, *nrp1b*, *nrp2a*, *nrp2b*, *robo2*, *robo3*, *sema3d*, or *dcc* all induce reliable but relatively low levels of guidance errors. The simultaneous loss of *nrp2b* and *sema3d*, *nrp1a* and *dcc*, or *nrp2a* and *nrp2b* induce more frequent errors in the trajectories of the same axons than either single mutant alone. It is easy to picture the sequential contributions that multiple axonal guidance cues make as an axon extends toward its target, encountering different cues as it advances (Comer et al., 2019; van Horck et al., 2004). In addition, many cues may simultaneously compete or cooperate to fine-tune pathway or target selection. The multiplicity of cues acting on a growth cone would provide some degree of robustness and also a mechanism for evolutionary change. Projections could be fine-

tuned or made more complex through the addition of guidance signals to those already in place. The differential expression of duplicated semaphorin and neuropilin genes in the zebrafish provide a fertile substrate for an evolutionary fine-tuning process.

**Conclusion**

We conclude that *nrp2a*, *nrp2b*, and *sema3fa* are each required for the exclusion of TRPC2-class OSNs from OMP-specific protoglomeruli in the developing olfactory bulb. This function is mediated through a shared pathway with *sema3fa* likely acting as a repellent ligand for TRPC2-class OSNs expressing *nrp2a* and/or *nrp2b*, altering growth cone behavior and constraining the sample space of TRPC2-class OSN axons. *Nrp2a* and *nrp2b* play partially redundant and parallel roles in this context. The relative severity of misprojection phenotypes suggests that additional cues, likely other class-3 semaphorins, act through *nrp2a* and *nrp2b* to affect TRPC2-class axon pathfinding. These findings are consistent with a model in which a robust, partially redundant mechanism of multiple cues cooperate to influence the trajectory of individual axons, without a single cue being decisive.

**Abbreviations**

CZ: Central zone; dpf: Days post fertilization; DZ: Dorsal zone; hpf: Hours post fertilization; LG1: Lateral glomerulus 1; LG2: Lateral glomerulus 2; LG3: Lateral glomerulus 3; LG4: Lateral glomerulus 4; MG: Medial glomerulus; OB: Olfactory bulb; OE: Olfactory epithelium; OP: Olfactory plexus; OR: Odorant receptor; OSN: Olfactory sensory neuron; VPG: Ventral posterior glomerulus;

**Acknowledgements**

45

**Authors' contributions**

RC performed *nrp2a* protoglomerular targeting experiments (Fig. 2), *nrp2a*;*nrp2b* double mutant experiments (Fig. 3), image segmentation (Fig. 1 and 6), *sema3fa*;*sema3fb* double mutant experiments (Fig. 4),  *nrp2b*;*sema3fa* double mutant experiments (Fig. 5), and live imaging experiments (Fig. 6). PD performed RNA-seq experiment (Fig. 1). AT performed *in situ* experiments (Fig. 1). YM performed *sema3fa* protoglomerular targeting experiments (Fig. 2). VP performed 6dpf *nrp2a*;*nrp2b* double mutant experiments (Fig. 3). XS performed *nrp2b* protoglomerular targeting experiments (Fig. 2). EZ performed *nrp2a*;*sema3fa* double mutant experiments (Fig. 5). RC and JR conceived the project, designed the experiments, and analyzed the data. RC and JR wrote the manuscript. All authors read and approved the final manuscript.

# Figure 1



**A**

OMP:RFP;TRPC:Venus

LG3, LG1, MG, LG2, DZ, CZ, LG4, VPG, OP

**B**

| Gene | OMP cpm (SEM) | TRPC cpm (SEM) | Fold Change | Adjusted p-value |
|---|---|---|---|---|
| nrp2a | 25.37 (2.40) | 112.65 (15.61) | 5.90 | 7.68E-10 |
| nrp2b | 52.37 (9.00) | 157.95 (17.94) | 4.08 | 9.89E-07 |
| sema3fa | 24.71 (6.13) | 13.89 (1.83) | 1.78 | 0.80 |

**C**  TRPC:Venus
nrp2a nrp2b
5µm

**D**  TRPC:Venus
nrp2a nrp2b
5µm

**E**

| | OMP | TRPC2 |
|---|---|---|
| nrp2a | 19% (n=163 cells) | 69% (n=56 cells) |
| nrp2b | 23% (n=355 cells) | 54% (n=33 cells) |

**F**  OMP:Gal4;UAS:Citrine
sema3fa
5µm

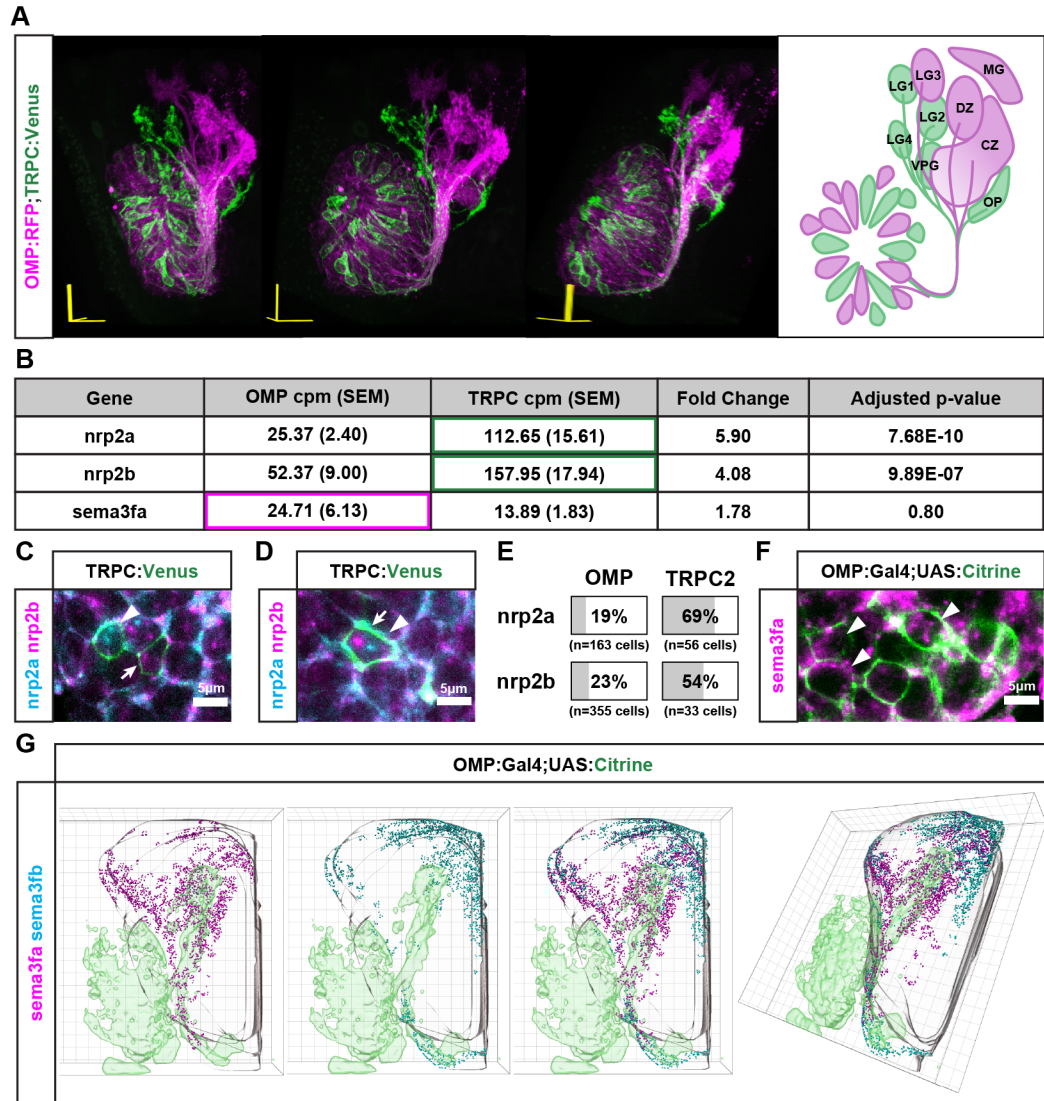**G**  OMP:Gal4;UAS:Citrine
sema3fa sema3fb

**Figure 1: Expression patterns of nrp2a, nrp2b, and sema3fa in the developing zebrafish olfactory system**

**A.** 3D projection and schematic representation (frontal view) of an optical z-stack of the 72 hpf olfactory system. One side of the olfactory system is shown with dorsal up and lateral on the left. OSNs are labeled by OMP:RFP (Magenta) and TRPC2:Venus (Green). OMP-expressing axons project to the central zone (CZ), dorsal zone (DZ), lateral glomerulus 3 (LG3), and medial glomerulus (MG). TRPC2-expressing axons project to the olfactory plexus (OP), lateral glomerulus 1,2, and 4 (LG1, LG2, LG4), and the ventral posterior glomerulus (VPG). **B.** RNAseq expression data from four replicate experiments for *sema3fa*, *nrp2a*, and *nrp2b* in OMP- and TRPC2-expressing OSNs. **C.** *Nrp2a* mRNA (cyan, arrowhead) and *nrp2b* (magenta, arrow) is detected independently in the cell bodies of TRPC2:Venus labeled cells (green) in the OE at 48 hpf. **D.** *Nrp2a* mRNA (cyan, arrowhead) and *nrp2b* mRNA (magenta, arrow) is detected in the same cell body of TRPC2:Venus labeled expressing cells (green) in the OE at 48 hpf. **E.** Percentage of OMP- and TRPC2-expressing cells with *nrp2a* or *nrp2b* expression. **F.** *Sema3fa* mRNA (magenta) is detected in the cell bodies of OMP:Gal4;UAS:Citrine expressing cells (green) in the OE at 48 hpf. **G.** *Sema3fa* and *sema3fb* expression in the olfactory system of 36 hpf zebrafish. 3D model of *sema3fa* mRNA  (magenta) and *sema3fb* mRNA (cyan) distribution within the OB (grey outline). *Sema3fa* is concentrated in the anterior and dorsal-medial regions of the OB and *sema3fb* is concentrated in the dorsal-medial regions of the olfactory bulb. Data aggregated from 6 OB hemispheres for *sema3fa* and 6 OB hemispheres for *sema3fb*.

**Figure 2**
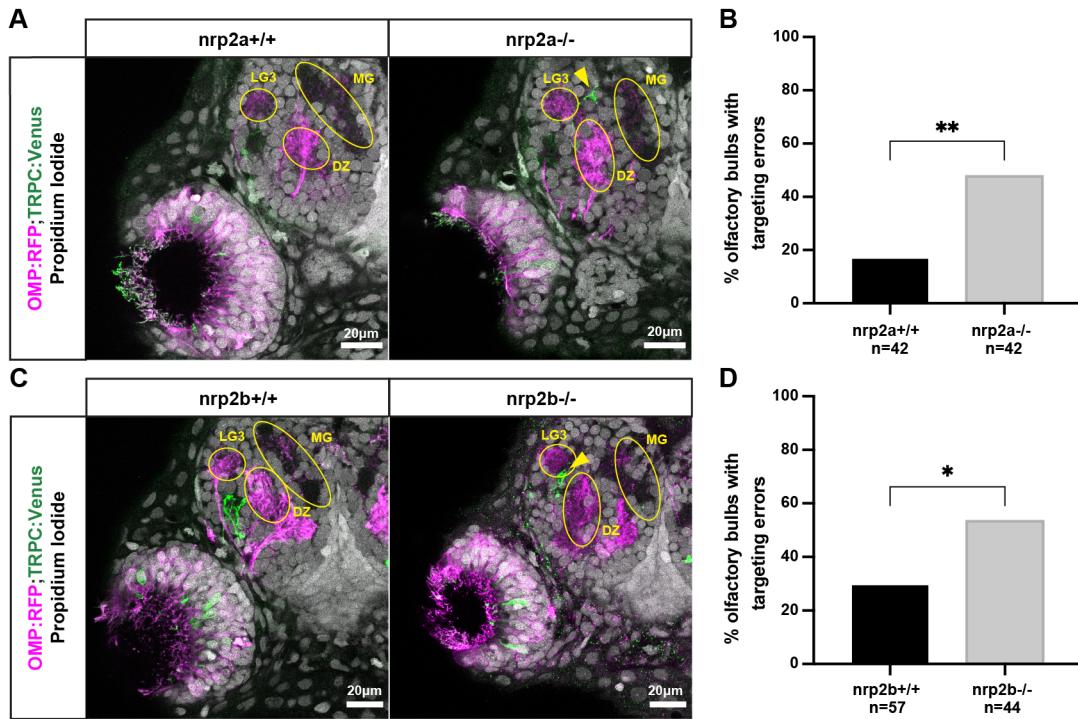


**Figure 2: Nrp2a and nrp2b are required for normal protoglomerular targeting of TRPC2-class OSNs**

**A.** Representative confocal sections of wild type and *nrp2a* mutant siblings. Yellow arrows indicate misprojecting TRPC2-class axons. **B.** The percentage of olfactory bulbs with targeting errors is higher in *nrp2a* mutants as compared to wild type siblings. **C.** Representative confocal sections of wild type and *nrp2b* mutant siblings. Yellow arrows indicate misprojecting axons. **D** The percentage of olfactory bulbs with targeting errors is higher in *nrp2b* mutants as compared to wild type siblings.

**Figure 3**



**Figure 3. *Nrp2a* and *nrp2b* likely work in parallel and targeting errors persist for days**

**A.** Representative confocal sections of 3 dpf wild type and *nrp2a;nrp2b* double mutant siblings showing multiple misprojections by TRPC2-class OSNs in the MG, DZ, and LG3 protoglomeruli. Yellow arrows indicate misprojecting axons. **B.** TRPC2-class OSNs in *nrp2a;nrp2b* double mutants project axons to more ectopic termination sites than single mutant or wild type siblings. **C.** Representative confocal sections of 6 dpf wild type and *nrp2a;nrp2b* double mutant siblings showing multiple misprojections by TRPC2-class OSNs in the MG and LG3 protoglomeruli. Yellow arrows indicate misprojecting axons. **D** Targeting errors of TRPC2-class OSNs persist into later stages of development. The number of ectopic termination sites per olfactory pit is significantly higher in *nrp2a;nrp2b* double mutant as compared to wild type siblings at both 3 dpf and at 6 dpf.
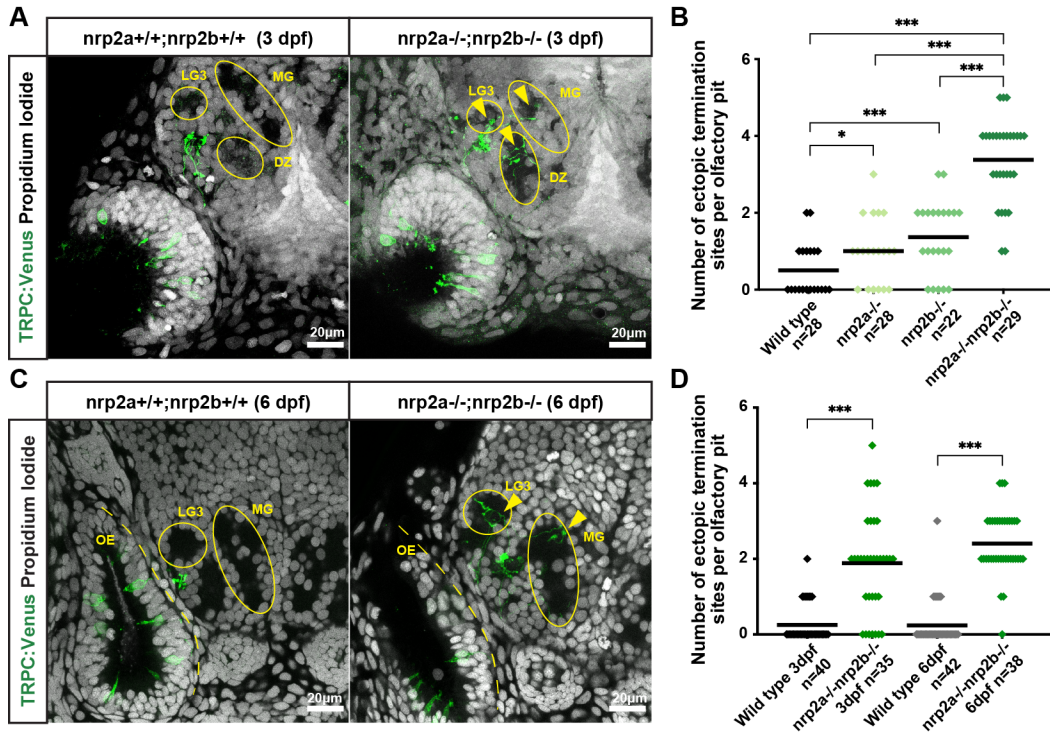
**Figure 4**

**A**



**B**



**C**
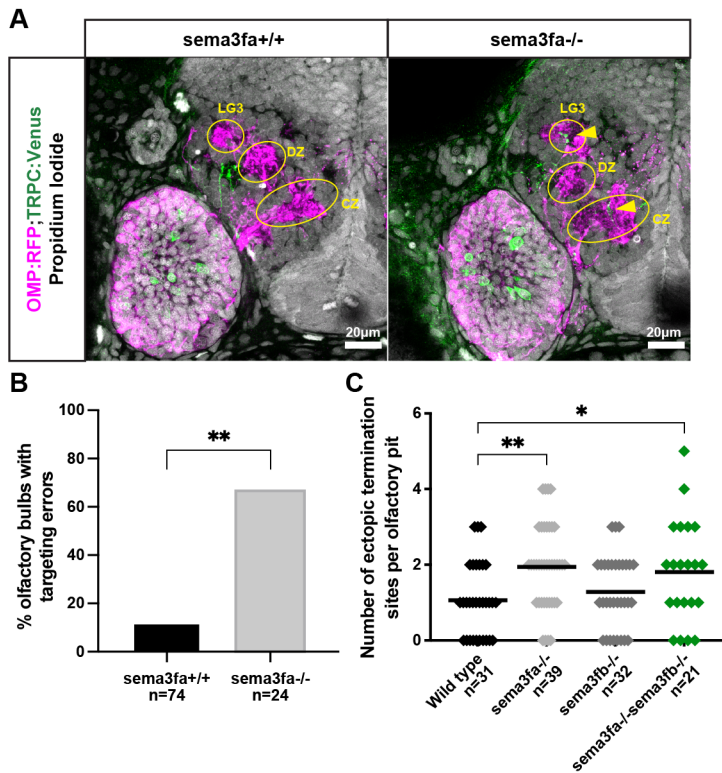


**Figure 4: *Sema3fa* is required for normal TRPC2-class OSN protoglomerular targeting**

**A.** Representative confocal sections of wild type and *sema3fa* mutant siblings. Yellow arrows indicate misprojecting axons. **B.** The percentage of olfactory bulbs with targeting errors is higher in *sema3fa* mutants as compared to wild type siblings. **C.** The misprojection phenotype of *Sema3fa* mutants is not significantly different from *sema3fa*;*sema3fb* double mutants.

51
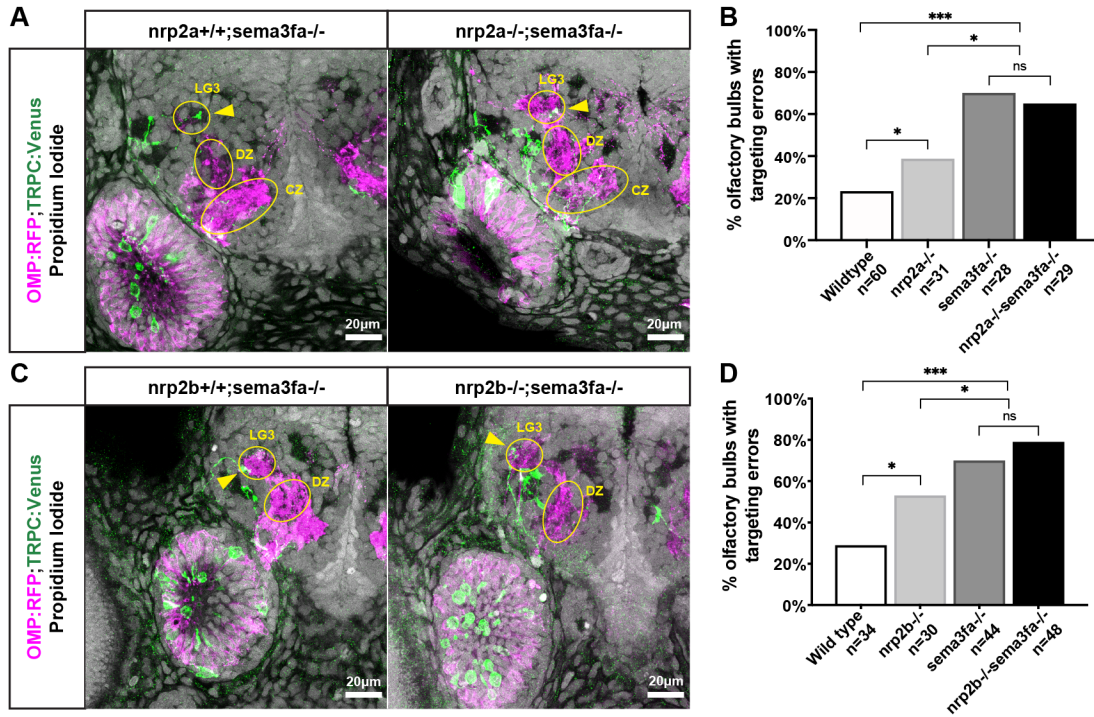
**Figure 5**



**Figure 5: Both *nrp2a* and *nrp2b* act in the same pathway with *sema3fa***

**A.** Representative confocal sections of *sema3fa* mutant and *nrp2a;sema3fa* double mutant siblings. Yellow arrows indicate misprojecting axons. **B.** The misprojection phenotype in *nrp2a;sema3fa* double mutants is not significantly different from *sema3fa* mutant siblings. **C.** Representative confocal sections of *sema3fa* mutant and *nrp2b;sema3fa* double mutant siblings. Yellow arrows indicate misprojecting axons. **D.** The misprojection phenotype in *nrp2b;sema3fa* double mutants is not significantly different from *sema3fa* mutant siblings.
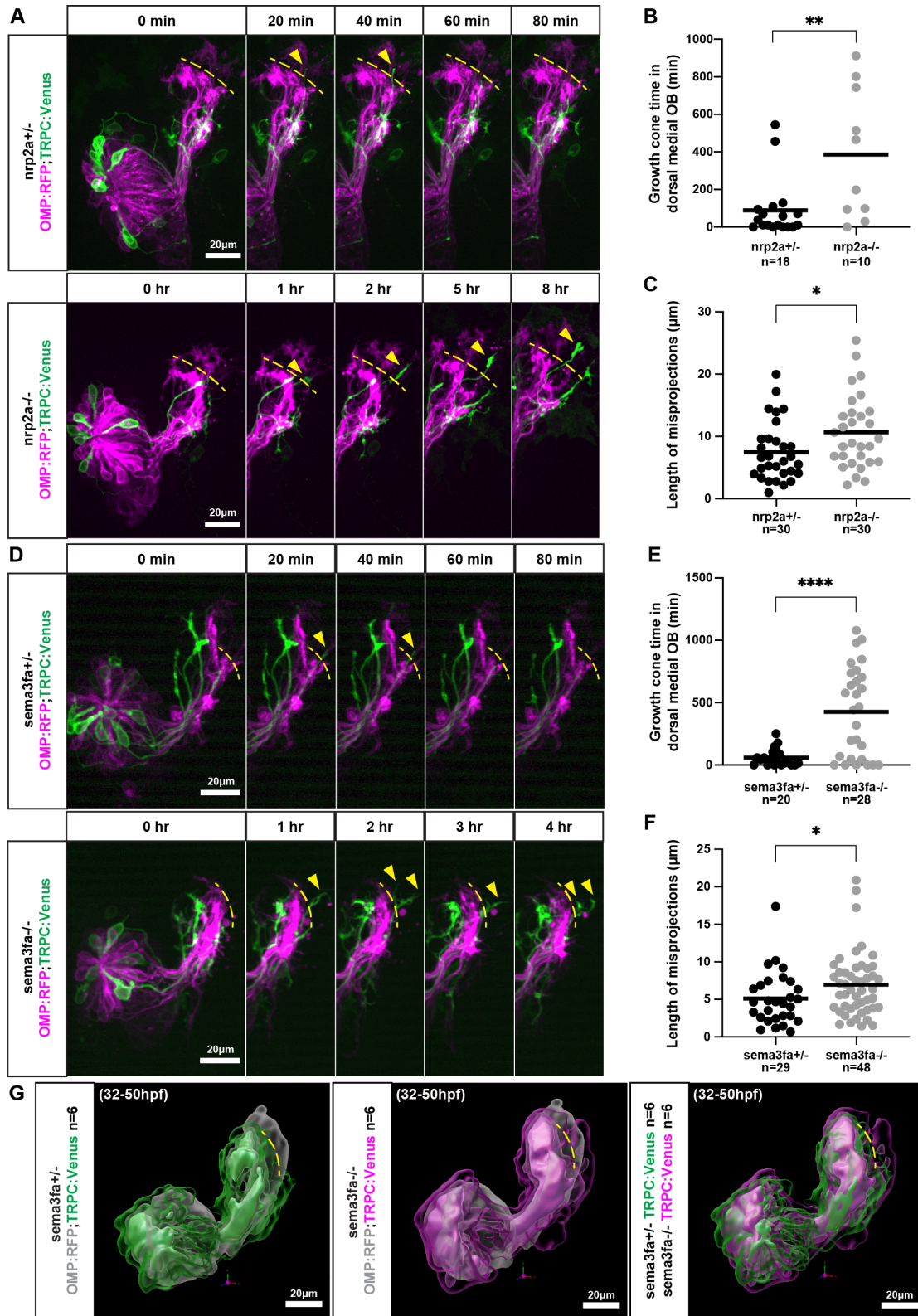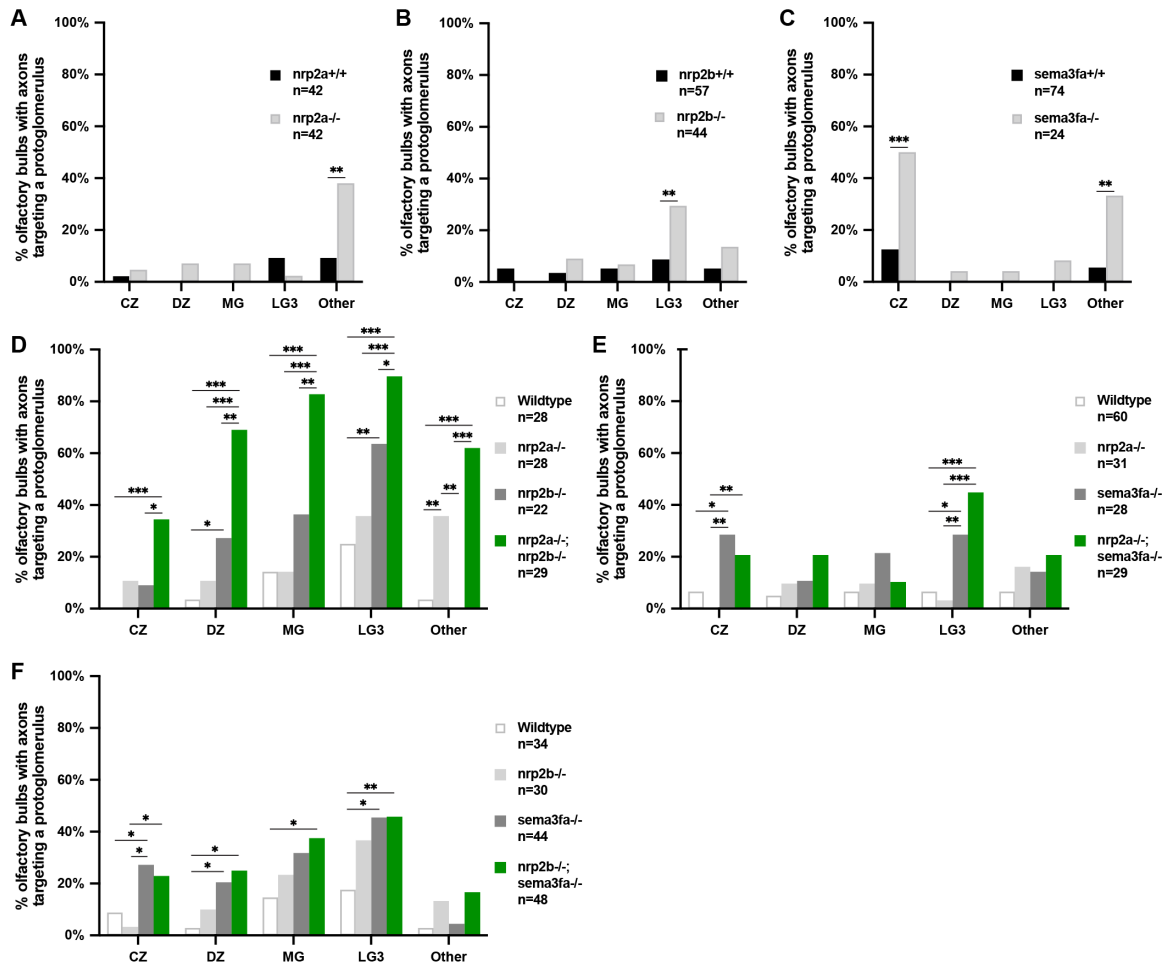
# Figure 6



53

**Figure 6: Misprojecting growth cones fail to retract in *nrp2a* and in *sema3fa* mutants**

**A.** Live imaging sequences of *nrp2a* heterozygote and mutant siblings, showing misprojecting axons occupying the dorsal-medial OB. The yellow dotted lines indicate the dorsal boundary of the developing DZ and CZ protoglomeruli and denote the edge of the dorsal-medial OB region. Yellow arrows indicate misprojecting axons. **B.** The cumulative time that the dorsal-medial OB is occupied by TRPC2-class OSNs is greater in *nrp2a* mutants as compared to *nrp2a* heterozygous siblings. **C.** The maximum distance TRPC2-class axons project into the dorsal-medial OB is greater in *nrp2a* mutants as compared to heterozygotes. **D.** Live imaging sequences of *sema3fa* heterozygote and mutant siblings, showing misprojecting axons occupying the dorsal-medial OB. **E.** The cumulative time that the dorsal-medial OB is occupied by TRPC2-class OSNs is greater in *sema3fa* mutants as compared to heterozygous siblings. **F.** The maximum distance TRPC2-class axons project into the dorsal-medial OB is greater in *sema3fa* mutants as compared to heterozygotes. **G.** Model of average TRPC2-class axon locations in *sema3fa* heterozygotes and mutants during live imaging sequence. TRPC2-class axons are shown in green and magenta, and OMP-class axons in grey. The three TRPC2 surfaces encompass axon location probabilities, from most transparent to most opaque, of 5.6%, 18.7%, and 31.8%. Yellow dotted line represents the edge of the dorsal-medial OB region.

**Supplemental figure 1: Quantification of misprojections**

**A.** Pattern of misprojections of TRPC2:Venus expressing OSNs in *nrp2a* mutants and wild type siblings. **B.** Pattern of misprojections of TRPC2:Venus expressing OSNs in *nrp2b* mutants and wild type siblings. **C.** Pattern of misprojections of TRPC2:Venus expressing OSNs in *sema3fa* mutants and wild type siblings. **D.** Pattern of misprojections of TRPC2:Venus expressing OSNs in *nrp2a*;*nrp2b* double mutants, *nrp2a* single mutants, *nrp2b* single mutants, and wild type siblings. **E.** Pattern of misprojections of TRPC2:Venus expressing OSNs in *nrp2a*;*sema3fa* double mutants, *nrp2a* single mutants, *sema3fa* single mutants, and wild type siblings. **F.** Pattern of misprojections of TRPC2:Venus expressing OSNs in *nrp2b*;*sema3fa* double mutants, *nrp2b* single mutants, *sema3fa* single mutants, and wild type siblings.

**Additional file 1.mov**

**3D projection of a z-stack of a wild type 72 hpf olfactory bulb.** Green is

TRPC2:Venus and Magenta is OMP:RFP. Z-stack was taken at 1 μm intervals.

**Additional file 2.mov**

**3D model of *sema3fa* and *sema3fb* mRNA distribution within the OB at 36 hpf.**

Magenta spheres represent *sema3fa* mRNA, cyan spheres represent *sema3fb* mRNA,

green structure represents OMP:Gal4;UAS:Citrine expressing OSNs, and grey structure

represents the OB.

**Additional file 3.mov**

**Maximum projection of time-lapse live imaging z-stack showing a *nrp2a+/-***

**olfactory hemisphere.** Green is TRPC2:Venus and Magenta is OMP:RFP. Time-lapse

starts at 32 hpf and continues for 680 minutes, at 10 minute intervals. Z-stack was taken

at 1 μm intervals.

**Additional file 4.mov**

**Maximum projection of time-lapse live imaging z-stack showing a *nrp2a-/-***

**olfactory hemisphere.** Green is TRPC2:Venus and Magenta is OMP:RFP. Time-lapse

starts at 32 hpf and continues for 680 minutes, at 10 minute intervals. Z-stack was taken

at 1 μm intervals.

**Additional file 5.mov**

**Maximum projection of time-lapse live imaging z-stack showing a *sema3fa+/-***

**olfactory hemisphere.** Green is TRPC2:Venus and Magenta is OMP:RFP. Time-lapse starts at 32 hpf and continues for 680 minutes, at 10 minute intervals. Z-stack was taken at 1 μm intervals.

**Additional file 6.mov**

**Maximum projection of time-lapse live imaging z-stack showing a *sema3fa-/-* olfactory hemisphere.** Green is TRPC2:Venus and Magenta is OMP:RFP. Time-lapse starts at 32 hpf and continues for 680 minutes, at 10 minute intervals. Z-stack was taken at 1 μm intervals.

**Chapter 3: Building a map of axon guidance cues in the developing olfactory bulb**

**Introduction**

The spatial regulation of gene expression is essential for biological function. Expression atlases for the major model systems have been developed and proven useful for hypothesis generation (Armit et al., 2017; Kalafatakis et al., 2020; Kunst et al., 2019; Richardson et al., 2014; Ronneberger et al., 2012; Yemini et al., 2021). Multiple atlases of the zebrafish brain have been created (MapZeBrain, Z-Brain, ZBB) and developed at the scale of the whole brain, and are useful for studies at the scale of brain regions. However, an expression atlas of the developing OB at the resolution or scale useful for olfactory axon guidance does not yet exist. The goal of this project is to create protocol to register expression information onto a model of the developing zebrafish OB.

Many classical guidance cues have been shown to be expressed in the developing OB, including eight class 3 semaphorins, two netrins, and four slits (Brose and Tessier-Lavigne, 2000; Kennedy, 2000a, 2000b; Lakhina et al., 2012; Miyasaka et al., 2005; Taku et al., 2016). Our lab has generated a large amount of *in situ* hybridization expression data for a wide range of axon guidance related genes in the OB. These datasets have informed our thinking about how OSN pathfinding is regulated. Models of how *Netrin/Dcc* and *Nrp1a/Sema3d* signaling guide *or111-17* transgene-expressing OSNs were proposed based on a combination of mutant phenotype analysis and expression pattern of guidance cues within the bulb (Lakhina et al., 2012; Taku et al., 2016). Additional receptors such as *robo2*, *nrp1b*, and *nrp2b* are also required for protoglomerular targeting (Dang et al., 2018; Taku et al., 2016). These studies, in addition to the experiments presented in chapter 2, suggest that OSN axon guidance

likely involves multiple sets of guidance/receptor pairs working in conjunction to organize the protoglomerular and glomerular map.

A leading hypothesis of OSN guidance in drosophila suggests that multiple guidance cues function simultaneously as a combinatorial code to guide each OSN (Hong and Luo, 2014). This hypothesis predicts that the overlapping guidance mechanisms provide redundancy and robustness to the system. The redundancy and robustness make such a system difficult to test on a gene-by-gene basis. A comprehensive atlas of the guidance cue landscape could help to model OSN guidance and generate more precise and testable predictions of guidance phenotypes.

One longstanding challenge has been the communication of the spatial patterns of guidance cue expression. It is difficult to visualize their expression patterns in 3D space and tricky to compare spatial distributions of different gene products. To solve these problems, I developed a model of the 36hpf zebrafish OB onto which expression data can be mapped. At this stage in development, OSN axons have arrived at the OB and are beginning to project to the sites of the developing protoglomeruli. *In situ* hybridization experiments show that many guidance cues are strongly expressed in the OB at this stage, including many class 3 semaphorins and netrins. As new genes are studied, they can be added to this model. This will enable us to visualize the environment through which OSN axons navigate to their protoglomerular targets.

A similar approach was first used in drosophila to create a quantitative probability map of olfactory projection neuron (PN) synapses in higher order olfactory centers (Jefferis et al., 2007). Using a sequential rigid and non-rigid autonomous registration algorithm, the authors were able to register over 200 samples, each with a single labeled PN, based on

brain morphology. The registered samples were used to map the synaptic connections

of 35 classes of PNs in the drosophila olfactory system. The result is a quantitative

connectivity map between the glomeruli of the OB and the neuropil of the mushroom

body and the lateral horn.

Zapiec and Mombaerts (2015) used 3D modeling and registration of multiple samples to

assess the positions of OR-specific glomeruli in the mouse OB . To answer the question

of how precise and stereotyped OR-specific glomeruli are, they used serial two-photon

tomography and multiplex genetic labeling of four or five OR-specific glomeruli. The

serial two-photon tomography technique produces 3D images of the olfactory bulb with

minimal distortion. The authors showed that a combination of uniform scaling and rigid

alignment was sufficient to register OBs from the left and right hemispheres of the same

animal, OBs of littermates, and OBs of animals at different ages. With the multiplexed

labeling of ORs providing an internal control for relative glomerular positions, the authors

convincingly demonstrated that the glomerular positions were well registered based only

on the rigid alignment.

In the previous chapter, expression models created by manual image-image registration

were presented. In this chapter, I present a protocol to improve on this technique and

facilitate model-image registration upon which future expression datasets can be built.

**Results**

**Custom alignment script for midline registration**

Landmark registration is a commonly used way to standardize the orientation of multiple

sample datasets. After manually annotating landmarks on each sample, the samples can

be manipulated to minimize difference in landmark positions between all datasets. This method of linear registration is often used as an initial optimization step for further non-linear registration methods. The linear registration helps to constrain the search space and enhances the chances of an accurate registration. We tested landmark registration algorithms on our *in situ* datasets but ran into issues with implementation. We were unable to identify landmarks in 36hpf OB datasets that could produce reliable registration.

While we were not able to identify enough precise landmarks for full registration, we found that the midline can serve as a critical landmark feature. Alignment of the midline planes of different samples greatly constrains the degrees of freedom during subsequent manual registration, resulting in a more standardized result. To this end, I developed a custom midline alignment script to transform individual samples such that the plane of the midline is positioned in a standardized fashion (Appendix). First, a buffer zone is added around the image on all six sides to ensure no information is lost when the image is rotated or translated within the z-stack. The script works by having the user define the midline-plane, which is easily identifiable in nuclear stained samples, by marking it at three random points. The sample is then rotated around all three axes to bring the midline-plane parallel to the YZ-plane. The position of the midline along the x-axis is determined, and the image is translated along the x-axis such that the midline is positioned at a standardized location on the x-axis. Using this script, a user can quickly and reliably reorient 3D image samples such that the midlines are all superimposed in the same location. Prior to alignment, there are obvious variations in the positioning and orientation in the data (Fig. 7A-D). Variations are seen both in the midline position as well as in the relative angle of the AP axis to the z-axis of the image, leading to differing

positions of the OE (Fig 7D). After processing through the alignment script, the same samples become much better aligned (Fig 7A-D).

**Creation of a reference model of the 36hpf zebrafish OB**

To aggregate expression data from different experiments, a reference model is needed as a template for alignment and display of the data. Data generated from 36hpf OMP:Gal4;UAS:Citrine larvae was used to create a reference model of the developing OB. Six samples were processed through the alignment script and imported into Imaris. The samples were then manually aligned based on OMP:Gal4;UAS:Citrine signal only by rotation in and translation along the YZ-plane to achieve a best fit while maintaining the position of the midline. A reference OB was created by drawing contour lines based on the average position of the registered OB samples, and a representative OMP:Gal4;UAS:Citrine sample was chosen and segmented to use as the reference OMP class-OSNs (Fig 8A). The signal of the six OMP:Gal4;UAS:Citirine samples are well registered, suggesting that the reference model is accurate (Fig 8B).

To test whether the reference models of the OB and OMP-class OSNs were sufficient for registration of new confocal z-stacks, four *sema3aa in situ* datasets were used for registration. The datasets were processed using the alignment script and imported into Imaris for further alignment. The alignment script ensured that midlines of all four samples were aligned in the same plane as the midline of the OB model. To align the OMP:Gal4;UAS:Citrine signal to the OMP-class OSN model, manual alignment was constrained to translation along the y- and z-axes and rotation around the x-axis. *In situ* hybridization signals of the aligned images were segmented to create models of *sema3aa* expression (Fig 8C). The expression models from the four samples line up

quite well, showing a concentration of expression in the middle of the OB hemisphere

posterior to the OSNs as well as in the dorsal-medial OB. The close alignment of *in situ*

signals from the four samples demonstrates that the OB and OSN models and alignment

protocol are sufficient for accurate alignment of z-stacks images of *in situ* hybridization

data.

**Multiple guidance cues are expressed in distinct patterns in the developing OB**

With a validated alignment protocol, I integrated the expression data of four other

guidance cues into the reference OB model. Four *in situ* samples each for *sema3fa*,

*sema3fb*, *ntn1a*, and *ntn1b* were aligned and segmented using the same protocol as

*sema3aa.* The segmented *in situ* signals from all four samples of each gene were

combined. The combined signal was filtered for outliers based on the average distance

of each segmented spot to its nearest nine neighbors. In Imaris, the distance

measurement is displayed as a frequency distribution, allowing the user to define a

cutoff. This filtering technique results in a spatial representation of the most concentrated

expression detected in multiple samples. After processing, the expression model for

*sema3aa* shows the same spatial distribution seen in the unfiltered model with less

noise. Expression is concentrated in the middle of the OB posterior to the OSNs as well

as in the posterior dorsal-medial OB (Fig 9A). *Sema3fa* expression is seen in the

anterior OB surrounding the OMP expressing OSNs, while *sema3fa* expression is

concentrated in the anterior dorsal-medial OB (Fig 9B and C). The attractive guidance

cues *ntn1a* and *ntn1b* are both expressed medially near the OMP-class OSNs. *Ntn1a* is

concentrated more dorsally, occupying the space between the two regions of *sema3aa*

expression, as well as along the midline in the ventral OB (Fig 9D). *Ntn1b* expression is

also found along the midline in the ventral OB but mostly concentrated on the medial

side of the site where the olfactory nerve enters the OB (Fig 9E). When all these models are combined together, a complex patchwork of guidance cues within OB is shown (Fig 9F-H).

**Creation of protoglomerular map model based on elastic registration**

Although we were unable to use landmark-based registration techniques on early stage larvae, new useful landmarks have emerged in the developing OB by 72hpf. At this stage, protoglomeruli have developed and are quite stereotyped. Images created by staining nuclei at this stage of development have similar levels of gross detail as images generated by MRIs and CT scans of human brains. I used a template generation tool developed for use on human brain scans to create an unbiased template of the 72hpf OB.

The symmetric group-wise normalization (SyGN) tool is a part of the Advanced Normalization Toolkit (ANTS) (Avants et al., 2009). The template generation method takes an unbiased, iterative approach to template generation. A group of samples are averaged to create an initial template onto which each sample is mapped based on a cross-correlation algorithm. The transformations determined in the mapping step are averaged to create a composite transformation and applied to create a new template. This process is iterated until the algorithm converges on a solution and creates an unbiased template.

To create a nuclear stain template of the 72hpf zebrafish OB, 20 confocal z-stacks of wild type larvae imaged at 1μm intervals were used as inputs. The z-stacks were processed through the antsMultivariateTemplateConstruction2.sh shell script in the ANTS software package. The resulting template shows clearly identifiable

protoglomeruli. Comparisons between samples before and after registration demonstrate a clear improvement in uniformity of protoglomerulus locations (Fig 10A). The image parameters for the construction of this template chosen to be compatible with the ones used in protoglomerular targeting experiments described in chapter 2. This allows for the template be used in future protoglomerular targeting experiments as a registration template.

With a consensus template of the zebrafish OB in hand, I wanted to create a segmented model of the important structures in the OB. Fiji was used to manually segment the OE and OB in the template, and the segmented images were imported into Imaris for further processing. 3D models of the OE, the individual protoglomeruli, and a portion of the midline were created (Fig. 10B).

**Discussion**

OSN axon guidance during protoglomerular targeting is dependent on the expression of multiple guidance cues. Disruption of the pattern of guidance cue expression, whether by knockdown, knockout, or ubiquitous overexpression, can cause the misprojection of OSNs (Dang et al., 2018; Lakhina et al., 2012; Miyasaka et al., 2005; Taku et al., 2016). Despite the recognized importance of guidance cue expression in the OB, a comprehensive map of guidance cue expression has not been made. In this study, I present custom tools developed for the construction of a map of guidance cue expression in the developing zebrafish OB. By using a custom alignment script followed by manual alignment using Imaris, a reference model of the 36hpf zebrafish OB and OMP-class OSNs was constructed from six OB samples. Using this model, I demonstrate the feasibility of using image-model registration to align *in situ* hybridization

samples and extract expression data to construct a model of the 36hpf OB containing expression patterns for five guidance cues.

The expression model described in this study is meant to be built upon. As more expression data are generated, they can be added to this model to create an increasingly comprehensive map of guidance cue expression. The expression models I have developed here work well to describe the spatial distribution of guidance cues within the OB. However, because of potential differences in segmentation and *in situ* detection thresholds, the model cannot be used to compare relative expression levels.

The cataloging of the guidance cue landscape faced by projection OSN axons will be useful both for hypothesis generation and for making sense of guidance phenotypes. This model is based on early stages of protoglomerular targeting, and we know that expression patterns change over time. *Robo2* expression is transient, increasing and decreasing over the span of 12 hours (Miyasaka et al., 2005). Expression of netrins is detectable at 36hpf and robustly expressed by 48hpf (Unpublished data). The methods described here could be used to construct reference models of the OB at later time points and will likely provide further insight into olfactory map formation.

While it has not been directly tested, it is expected that expression data generated by immunostaining will likely be compatible with the protocols and reference model presented here. *In situ* hybridization protocols can affect the structure of tissues and can lead to distortions in morphology. This can lead to problems when trying to align data generated through other protocols. Attempts to align data generated from live-imaging experiments to the reference model were unsuccessful, presumably because of the distortions caused by *in situ* hybridization represented by the model (data not shown).

These challenges could be overcome in the future by using non-rigid registration techniques. Currently, this has been computationally difficult to achieve. The major bottleneck is the lack of a useful signal for registration algorithms to act on. The OMP:Gal4;UAS:Citrine signal works well as a landmark for manual alignment but does not cover enough space within the dataset to provide robust alignment information for non-rigid registration. The nuclear stain signal at 36hpf occupies enough of the sample space but is too uniform throughout the dataset for registration algorithms to act on. I have shown here that with the correct signal, it is possible to algorithmically register OB datasets (Fig 10). For future experiments, a new marker gene could be identified and labeled using immunofluorescence to facilitate non-rigid registration. This registration algorithm also has the potential for automating phenotype analysis of protoglomerular targeting. With increasing computing power, it may become possible to register protoglomerular targeting datasets such as the ones presented in chapter 2. This would allow for higher throughput of mutant analysis and facilitate the detection of infrequent guidance errors, a process that currently requires extensive training to do manually.

The modeling and registration of image data has potential uses in study of all manner of biological systems. It allows for the leveraging of large sample sizes to study complex or subtle phenotypes. Models of complex datasets can be used to make and test predictions that would otherwise be impossible. One example is the hypothesis that OSN axon guidance is determined by a combinatorial code of axon guidance receptor expression (Hong and Luo, 2014). In this proposed model of drosophila OSN axon guidance, multiple axon guidance receptors are expressed by each OSN. The cooperation of multiple guidance pathways regulates the precise axon guidance of the OSN and likely also confers a level of robustness to the axon targeting process. Based

on this hypothesis, knockouts of single genes are unlikely to result in severe disruption

of axon guidance as the other guidance mechanisms continue to function. Modeling and

registration can be useful here in a couple of ways. A comprehensive understanding of

the guidance cue landscape could be developed through modeling and registration.

Such a model could then be used to make more precise and testable hypothesis or

predictions around misprojection phenotypes, genetic interactions, and differential

behavior between different OSN populations. Modeling and registration can also be used

to analyze large numbers of samples, making it possible to study mild phenotypes that

are currently studied using modifier mutants. As imaging and other data collection

techniques continue to improve, we will need increasingly sophisticated techniques to

organize all the information being generated and leverage it to elucidate ever more

complex mechanisms.

**Figure 7**
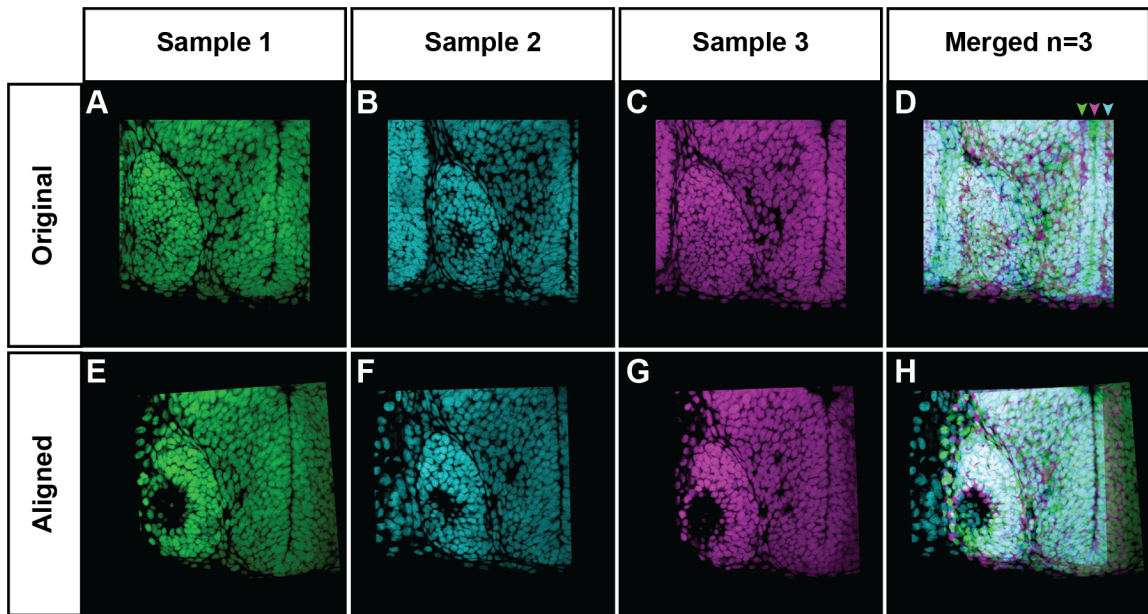


**Figure 7. Example results of custom alignment script**

**A-C.** Representative single optical slices from three z-stacks of 36hpf olfactory bulbs. Frontal view, dorsal is up, lateral is to the left. A black border has been added. **D.** Composite of single optical slices shown in **A-C**. Arrowheads indicate the midline from each sample. **E-G.** Representative single optical slices from the z-stacks shown in **A-C** after processing through alignment script. **H.** Composite of single optical slices shown in **E-G**.

**Figure 8**



| | Frontal view | Perspective view |
|---|---|---|
| **A** 36hpf reference model | | |
| **B** OMP:Gal4;UAS:Citrine n=6 | | |
| **C** sema3Aa mRNA n=4 | | |
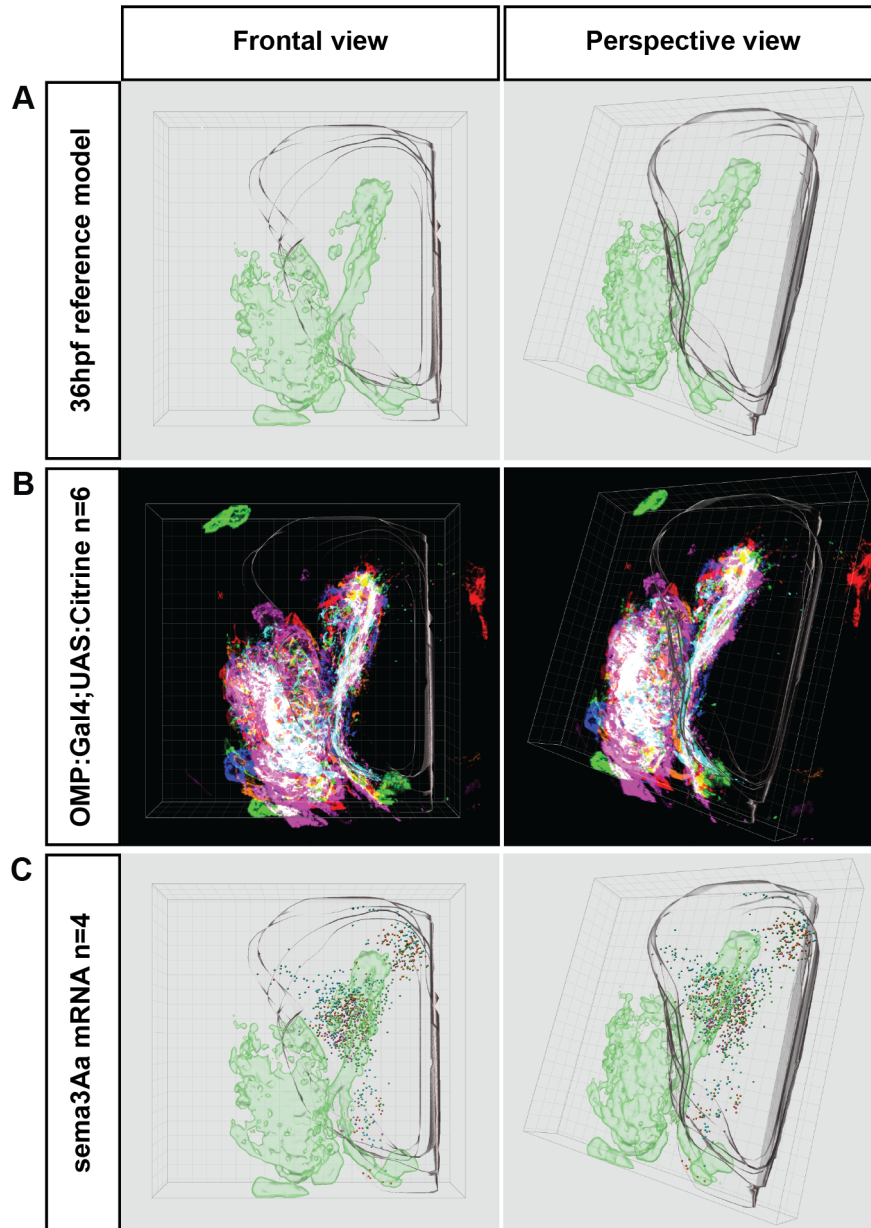
**Figure 8. Creation and validation of a reference model of the 36hpf zebrafish OB**

**A.** 3D model of a 36hpf zebrafish OB. A representative OMP:Gal4;UAS:Citrine signal is in green, marking the position of OMP-class OSNs. The transparent grey surface represents the consensus bounds of the OB hemisphere. **B.** OMP:Gal4;UAS:Citrine signal of the six aligned images used to generate the reference OB model shown in red, green, blue, cyan, magenta, and yellow. **C.** *sema3aa in situ* signal from four images aligned to the reference model (cyan, magenta, orange, and green).

**Figure 9**



sema3aa expression

sema3fa expression

sema3fb expression

A

B

C

netrin1a expression

netrin1b expression

D

E

sema3aa sema3fa sema3fb netrin1a netrin1b

F

G

H
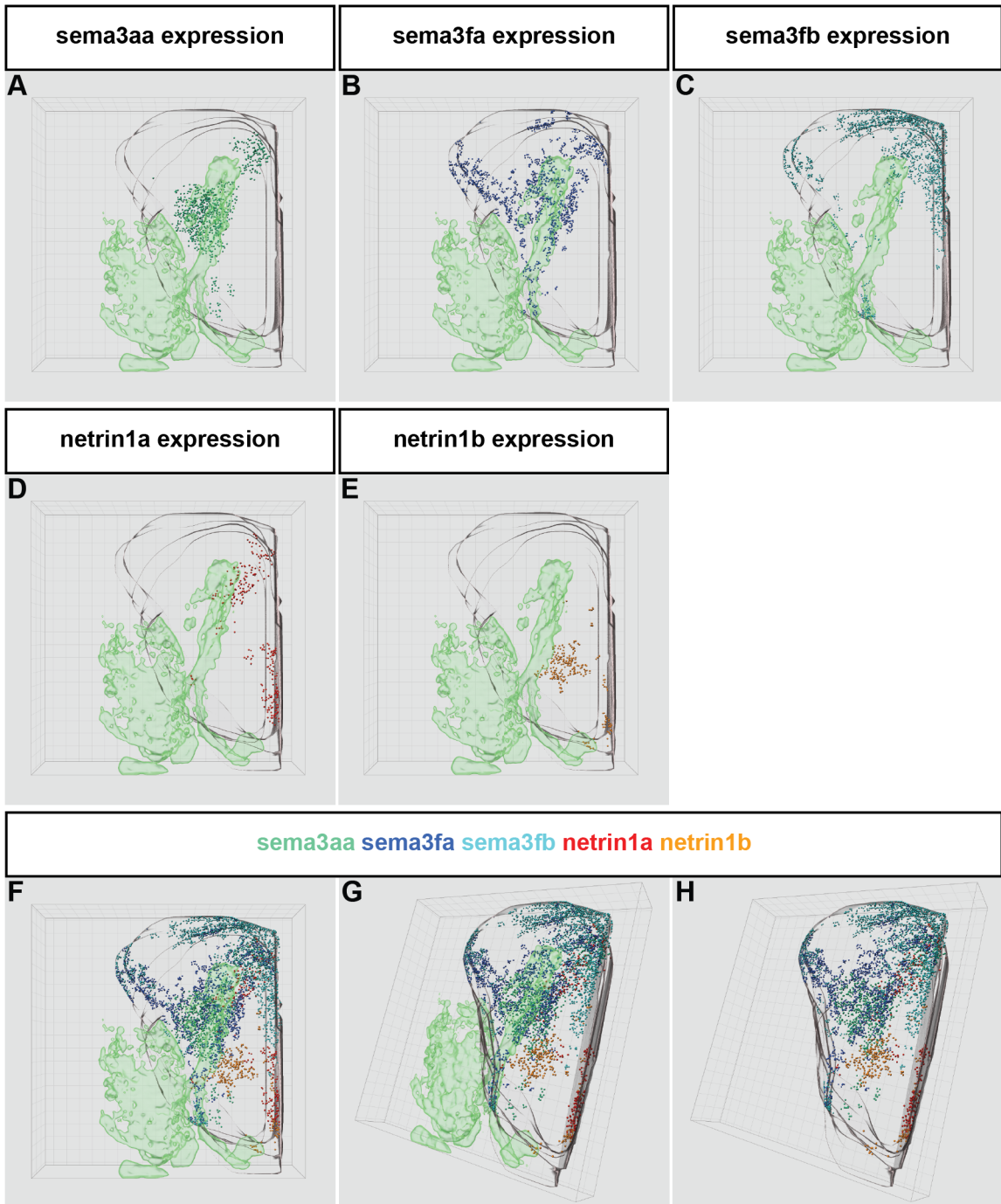
**Figure 9. Expression data modeling of attractive and repellent guidance cues in the 36hpf zebrafish OB**

**A.** Model of *sema3aa in situ* signal aggregated from four samples aligned to the 36hpf OB model. **B.** Model of *sema3fa in situ* signal aggregated from four aligned samples. **C.** Model of *sema3fb in situ* signal aggregated from four aligned samples. **D.** Model of *netrin1a in situ* signal aggregated from four aligned samples. **E.** Model of *netrin1b in situ* signal aggregated from four aligned samples. **F-H.** Frontal and perspective views of the 3D model of the 36hpf zebrafish OB showing expression of *sema3aa, sema3fa, sema3fb, netrin1a*, and *netrin1b*.

**Figure 10**
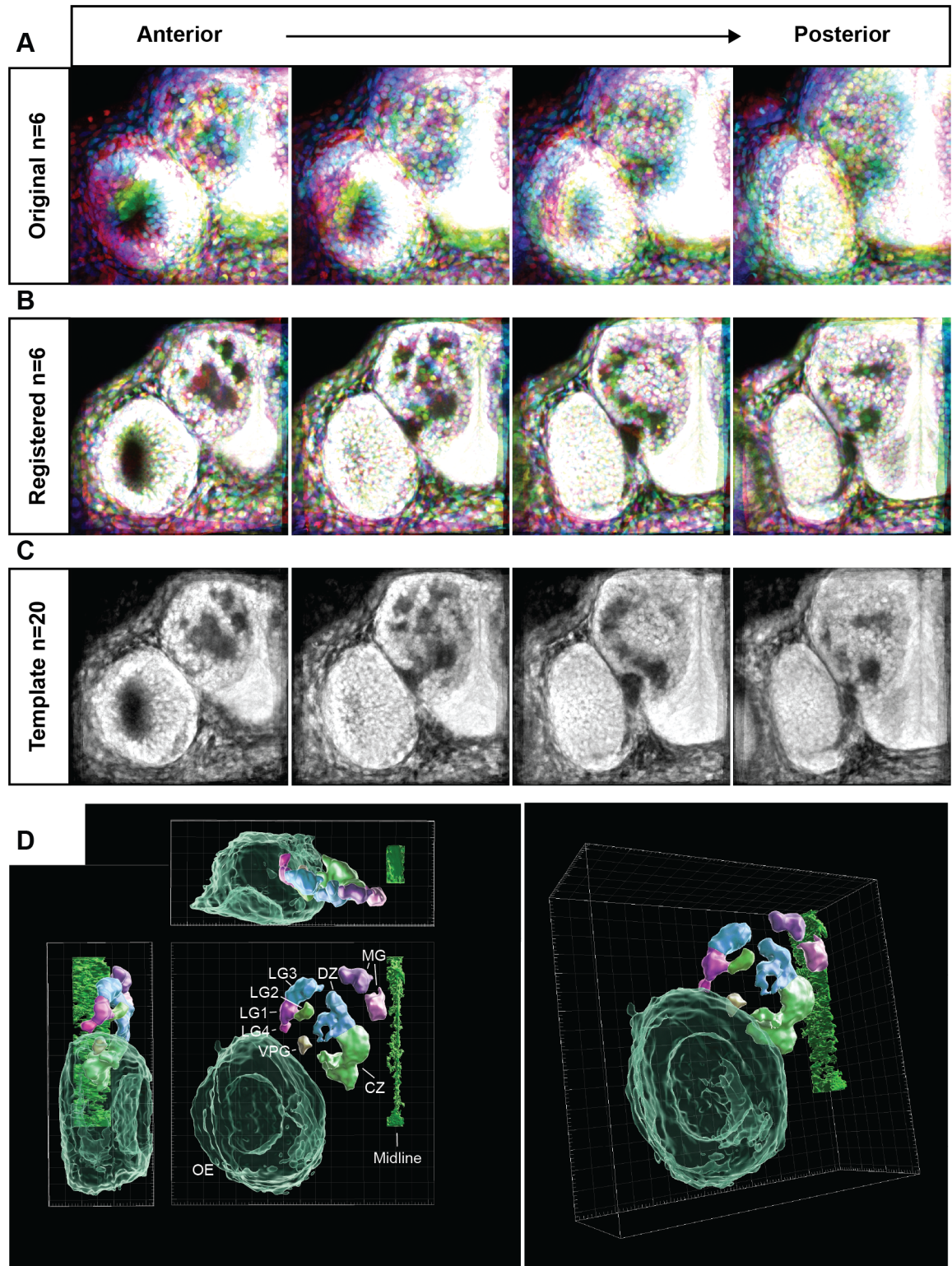
**Figure 10. Unbiased z-stack template and model of a 72hpf zebrafish OB**

**A.** Composite of six z-stack examples of nuclear-stained OBs of 72 hpf zebrafish used for template generation. Frontal view, dorsal is up, lateral is to the left. Each sample is set as a different color (red, green, blue, cyan, magenta, and yellow). Individual sections are arranged from anterior (left) to posterior (right) with 7μm between each section shown. **B.** Same six z-stack examples shown in **A** after registration in the template generation process. **C.** Single optical sections from an unbiased z-stack template generated from 20 z-stacks of nuclear-stained OBs of 72 hpf zebrafish. **D.** 3D model of a 72 hpf zebrafish OB segmented from the template in **C**. OE, protoglomeruli, and midline are labeled. Orthogonal views are shown on the left, diagonal view on the right.

**Chapter 4: Conclusion and future directions**

In the studies presented here, I have shown *nrp2a*, *nrp2b*, and *sema3fa* are required for normal protoglomerular targeting of TRPC2-class OSNs to TRPC2-specific protoglomeruli. In mutants for all three of these guidance factors, axons of TRPC2-class OSNs occasionally misproject into OMP-specific protoglomeruli. The guidance receptors *nrp2a* and *nrp2b* are expressed in partially overlapping subsets of TRPC2-class OSNs, while *sema3fa* is expressed by OMP-class OSNs and by cells in the OB. Genetic interaction experiments indicate that *nrp2a*, *nrp2b*, and *sema3fa* likely work in the same pathway with *sema3fa* acting as a repulsive ligand for OSNs expressing *nrp2a* and/or *nrp2b*. The severity of the *sema3fa* mutant phenotype compared to the *nrp2a;nrp2b* double mutant phenotype suggest that it is likely not the only ligand involved in *nrp2-* dependent protoglomerular targeting.

Using live imaging studies conducted at 10 minutes/frame, I show that, contrary to previous reports, OSN axons do not project directly to their targets but instead often extend and retract, sampling a large region of the OB over a period of hours. I find that axon growth cone behavior is affected in *nrp2a* and *sema3fa* mutants. In mutant animals, the area sampled by TRPC2-class OSNs is extended beyond the normal range, in particular, towards the dorsomedial region of the OB.

In these studies, a differential requirement for *nrp2* and *sema3f* guidance factor paralogs was observed. Knocking out *nrp2a* or *nrp2b* alone results in relatively mild but measurable phenotypes suggesting that they each have independent roles. When both nrp2 receptors are knocked out, a more severe misprojection phenotype is observed, exceeding the expected combined misprojection phenotype of *nrp2a* and *nrp2b* single

mutants. This suggests that *nrp2a* and *nrp2b* also have redundant functions in protoglomerular targeting of TRPC2-class OSNs. Experiments conducted with a presumptive *sema3fb* knockout allele did not show degraded protoglomerular targeting either in the presence or absence of sema3fa, suggesting that *sema3fa* is required in this context but *sema3fb* is not. Taken together, these results suggest that paralogs, even those in the same signaling pathway, can evolve to be semi-redundant, as with the *nrp2*s, or become independent and specialized, as with the *sema3f*s.

Together, these results add to the growing list of attractive and repulsive guidance cues involved in protoglomerular targeting. They also support a model in which a robust, partially redundant system of multiple axon guidance signaling pathways cooperate to regulate the protoglomerular targeting of individual OSN axons.

**Are there behavioral changes in mutants to biologically relevant odors?**

Experiments in mouse have shown that disruptions in olfactory circuit formation can result in changes in innate predatory avoidance and social behaviors (Cho et al., 2011; Inokuchi et al., 2017). Specifically, Robo2 deletion in OSNs cause mice to respond less to predator odors, while conditional knockout of Nrp2 in mitral cells impairs behavioral responses to attractive social signals (Cho et al., 2011; Inokuchi et al., 2017). Odor-based behavioral assays have been developed for both larval and adult zebrafish (Herrera et al., 2021; Kermen et al., 2020). Behavioral responses in larval zebrafish can be assayed both in free-swimming and in head-fixed experimental setups (Herrera et al., 2021). Free-swimming assays in which multiple test subjects are recorded simultaneously allow for relatively high throughput experiments. This facilitates the identification of mild differences in behavioral responses. Head-fixed experiments allow

for more controlled testing of different odors as well as simultaneous imaging of calcium signals in the brain. In adults, odor-induced behavior can be measured through the tracking of animals over time after the introduction of an odor stimulus (Kermen et al., 2020; Koide et al., 2009). Specific locomotive behaviors such as swimming velocity, freezing, abrupt turns, and burst swimming in response to different ecologically relevant odorants have also been characterized (Kermen et al., 2020).

It has been suggested that OSNs that project to the lateral glomeruli, such as the ones targeted by TRPC2-class OSNs, are responsible for attraction to amino acids (Koide et al., 2009). It would be interesting to test whether the misprojections caused in *nrp2a*, *nrp2b*, or *sema3fa* mutants have any behavioral consequences. Studies suggest that receptors expressed by TRPC2-class OSNs are sensitive to amino acids and nucleotides, odorants associated with feeding behavior (Friedrich and Korsching, 1998; Koide et al., 2009; Lipschitz and Michel, 2002; Luu et al., 2004). Ablation of OSNs that project to the lateral glomeruli (TRPC2 specific) abolishes the attractive response to amino acids by adult zebrafish (Koide et al., 2009). It is possible that misprojection of TRPC2-class OSNs would result in similar altered behavioral responses to food associated odorants. Whether misprojecting axons are capable of conveying odor stimuli or simply degrade the normal function of TRPC2-specific odor circuitry is also an interesting question. Since many of the guidance mutants in zebrafish can be grown to adulthood, it would be possible to test whether circuit formation phenotypes might be linked to altered behavioral response both in larvae and in adults. To clearly determine the role of axon guidance in behavior, better tools such as conditional mutants will need to be developed. Cre recombinase has been successfully used in zebrafish, and

improved CRISPR/Cas9 and PhiC31 knock-in techniques have made it feasible to construct conditional alleles (Almeida et al., 2021; Mosimann et al., 2011, 2013).

**What explains the resilience of OSN axon guidance to guidance cue knockouts?**

OSN axon guidance is surprisingly robust. In guidance factor knockout models, glomerular map formation is often only partially disrupted. Instead of a single shifted glomerulus, ectopic glomeruli are often formed in a distant location, in addition to glomeruli that appear to be in their stereotypical wild type positions. This type of duplicated organization of glomeruli have been seen in different knockout models in mouse, both in global and conditional knockout models, often with a subset of OSNs targeting what appears to be the wild type glomerulus (Assens et al., 2016; Cho et al., 2012; Imai et al., 2009; Takeuchi et al., 2010; Zapiec et al., 2016). In some instances, ectopic glomeruli were reported to be formed in expanded regions of the OB but anchored by the position of the wild type glomerulus (Zapiec et al., 2016). How is normal axon guidance maintained for the subsets of OSNs that still project to wild type positions under guidance cue knockout conditions? It has been proposed that OSNs expressing the same OR might express different guidance cues, thus explaining the multiple glomeruli seen when Nrp1 is deleted (Assens et al., 2016). It has also been suggested that the removal of a guidance cue lifts the constraints on axon projections, which overcomes the ability for later axon fasciculation mechanisms to form a single glomerulus (Takeuchi et al., 2010). This explanation fits with the observation that ectopic glomeruli tend to form in extended but defined regions of the OB around the original glomerulus (Zapiec et al., 2016). These explanations are not mutually exclusive. Another possibility is that altered cues are important for glomerulus formation but not protoglomerular targeting of axons in the OB. By analyzing glomerular location in

newborn mice, it is impossible to attribute shifted or altered glomeruli to either process. Investigation into earlier stages of glomerular map formation could clarify the underlying mechanisms.

The accessibility of the developing olfactory system makes zebrafish a much better model for studying early glomerular map formation compared to mouse. Similar to phenotypes seen in mouse, partial misprojection phenotypes are also seen in protoglomerular targeting of OSNs. In guidance factor mutants, significant subsets of OSNs continue to target the correct protoglomerulus. In *nrp1a*, *nrp2b*, and *sema3d* mutants, only a portion of *or111-7* transgene-expressing OSNs misproject to ectopic protoglomeruli. In *nrp1b* and *robo2* mutants, only a subset of *or130-1* transgene-expressing OSNs misproject from the DZ to the CZ protoglomerulus, while others maintain normal protoglomerular targeting (Dang et al., 2018; Taku et al., 2016). Similar partial misprojection phenotypes are seen with *or111-7* transgene-expressing OSNs when *ntn1a*, *ntn1b*, or *dcc* are knocked down (Lakhina et al., 2012). It is possible that glomerular formation can only happen within a protoglomerulus; thus, the ectopic glomeruli seen in mouse guidance cue knockout models could be the consequence of partial protoglomerular misprojections, splitting the population of OSNs to form two or more glomeruli. OSNs that project to the same protoglomerulus would likely be able to coalesce into a single glomerulus. Duplicated glomeruli within a tightly defined region such as a protoglomerulus would suggest that the affected guidance cues are important for glomerular segregation but not protoglomerular targeting. This hypothesis would fit with what was proposed by Takeuchi et al. (2010). However, this only moves the question one step forward.

What might explain the partial protoglomerular misprojection phenotype seen in zebrafish guidance mutants? One possible explanation for why only a subset of OSNs expressing the same OR misproject is that they do not express the same suite of axon guidance factors. OSNs expressing the *or111-7* transgenic OR have been shown to express all four of the zebrafish neuropilins. The expression the four neuropilins is not uniform. *Nrp1a* mRNA was detected in 66% of *or111-7* transgene-expressing OSNs, while *nrp1b*, *nrp2a*, and *nrp2b* were detected in 54%, 17%, and 46% of these cells, respectively. One explanation for the heterogeneity could be differing maturity levels within the labeled population. Another explanation is that the varied levels of expression of these guidance receptors are close to the detection threshold of the *in situ* hybridization protocol. However, it is also plausible that the heterogeneity seen in this population of cells could be indicative of differential guidance factor expression. *Nrp1a*, *nrp1b*, and *nrp2b* mutant phenotypes suggest that all three receptors play a role in the guidance OSNs expressing the same OR. A caveat here is that the expression profile of OSNs expressing a transgenic OR may not fully align with OSNs expressing the same OR from the endogenous locus.

Attraction meditated through *Ntn1b*/*Dcc* and repulsion through *Nrp1a*/*Sema3d* work in tandem to guide *or111-7* transgene-expressing cells to the CZ protoglomerulus in addition to *sema3d* independent axon guidance signals mediated through *nrp1b* and *nrp2b*. Clearly, multiple axon guidance cues play a role in the process of guiding a single OSN subtype to its target in the OB. Single cell RNAseq could be used to investigate the guidance cue expression profiles of OSNs expressing the same OR. Single cell expression profiling of these cell populations could be used to test for correlations

between guidance factor expression and maturity levels as well as to characterize the combinatorial expression of axon guidance cues.

Functional redundancy of axon guidance factors could also explain partial misprojection phenotypes. The experiments presented here (Chapter 2) suggest that the two *nrp2* paralogs in zebrafish have redundant functions in a large subset of TRPC2-class OSNs. Both paralogs respond to the same repulsive signals of *sema3fa* and knockout of either one results in partial misprojection phenotypes in protoglomerular targeting. It is possible that a dosage effect exists between the two paralogs in which the combined expression level of the two *nrp2*s is required for protoglomerular targeting. Alternatively, the partial phenotypes seen could be the result of differential requirements of *nrp2a* and *nrp2b* in different sub-populations of TRPC2-class OSNs. Genetic tools that label OSNs expressing *nrp2a* or *nrp2b* could be used to investigate the cell-autonomous effects of axon guidance receptor knockout on protoglomerular targeting.

A surprising finding from our live imaging experiments was the extent to which an individual OSN sampled the OB environment. It was previously suggested that OSNs projected directly to their targets in OB (Dynes and Ngai, 1998). Higher temporal resolution imaging has revealed that TRPC2-class OSNs can explore a relatively large area of the developing OB, with some axons sampling up to half of the OB hemisphere within the span of a few hours (Chapter 2). Future experiments could be done using genetic lines that label other subsets of OSNs. It would be interesting to investigate growth cone behavior in *or111-7* and *or130-1* transgene-expressing OSNs. Do these cells project directly to the CZ and DZ protoglomeruli, or do the growth cones sample different protoglomeruli before choosing their targets? The sample space of these OSNs could be determined by combining live imaging and registration. It is conceivable that a

map of sample spaces could be developed for OSNs expressing different OR subtypes or subfamilies.

Overall, it is notable how robust normal OSN axon guidance appears to be under axon guidance knockout conditions. The system is likely built on a multitude of overlapping redundant mechanisms. It will take careful measurement and analysis to further tease apart all the different systems involved.

**What is the guidance landscape of the developing olfactory bulb?**

Many guidance cues have been identified to play a role in OSN axon guidance to the vertebrate OB. The specific localization of these guidance cues along the path of axon guidance or at the target site is thought to be essential for the function of these mechanisms. Despite the recognized importance of spatial patterning of guidance cues, a comprehensive map of guidance factors has yet to constructed.

Many classical guidance cues are expressed in the developing zebrafish olfactory system. Two netrins, eight class 3 semaphorins, and four slits are expressed in various patterns and time points within the OB and by OSNs. Only a subset of these have been tested for their involvement in OSN axon guidance, but the specific expression patterns suggest that they likely play a role in the axon guidance process.

Expression patterns in the OB have been challenging to describe. Without easy landmarks for reference, it has been difficult to rigorously define locations or an accurate AP axis within the OB (Zapiec et al., 2016). In the mouse, it was reported that a Nrp1 gradient existed along the AP axis of the medial OB (Imai et al., 2006). The development of an exhaustive model of Nrp1 expression at every glomerulus in the mouse MOB

challenged whether the previously reported Nrp1 gradient along the medial OB was sufficient to regulate glomerular map formation along the AP axis (Zapiec et al., 2016).

Good registration and modeling have played an important role in studies of the olfactory system. The precise mapping of glomerular locations and demonstration of the stereotypy of OR specific glomeruli was achieved by a combination of multiplex expression of labeled OR alleles and registration of multiple OB samples (Zapiec and Mombaerts, 2015). Registration and multiplex mapping of OR gene expression was used to develop a more comprehensive and detailed understanding of OR expression zones in the OE as well as the projection domains of two classes of OSNs (Zapiec and Mombaerts, 2020). The projectome of the zebrafish OB was mapped using a combination of single cell labeling and elastic registration (Miyasaka et al., 2009, 2014). By using registration signals detected from multiple animals, experiments could be combined for more comprehensive analysis.

A comprehensive mapping of guidance cues in the developing OB will be useful in untangling the complex guidance mechanisms that form the glomerular map. It will facilitate the development of testable predictions, especially since multiple guidance cues are likely to be functioning at the same time. Overlaying OSN projection patterns for different subsets of OSNs, both in wild type and guidance cue knockout conditions, will no doubt give us further insight into the mechanisms behind protoglomerular map formation.

In this thesis, I have uncovered roles for *nrp2a*, *nrp2b*, and *sema3fa* in the protoglomerular targeting of TRPC2-class OSNs and showed that these guidance factors function to regulate the sample space of projecting OSN axons. I have developed

protocols for the registration and mapping of guidance cue expression, modeling of

protoglomeruli, and quantification of live-imaging data of axon projections in the

developing OB. The techniques and templates described in this thesis provide a

framework for investigating the complex combination of guidance factors involved in

protoglomerular and olfactory map formation.

APPENDIX

**Custom midline alignment script**


**Language: IJ1 Macro**


```
//This macro is used for preprocessing of in situ data sets to be
used for in situ modeling on Imaris
//Data files should be saved as .tif z-stacks prior to use with
this script
//The macro is designed to be used on z-stacks of in situ
hybridization samples or samples from immunostaining
//Samples should include propidium iodine or other types of
nuclear staining
//Designed for 1024x1024 images. Should work fine for smaller
images. For larger images sizes, make adjustments to addBorder()
to increase border size
//

//Hard coded parameters (Final position of the midline, size of
buffer zone to add to image)
midlinePixel = 1124
borderSize = 200
bufferSlices = 20

//Main script
//All functions are shown and annotated bellow
mirrorImage();
addBorder(borderSize, bufferSlices);
getMidlinePoints(bufferSlices);
rotate();
translateMidline();



//Left-right mirroring
//Asks user to if image orientation is correct. Flips image
horizontally depending on user response.
function mirrorImage (){
items = newArray("Yes", "No");
setSlice(nSlices/2);
Dialog.create("Mirroring");
Dialog.addMessage("Is the OE on the left and OB on the right?");
Dialog.addChoice(" ", items);
Dialog.show();
choice = Dialog.getChoice();

if (choice == "No") {
     run("Flip Horizontally");
```

```
        }

    }

    //Add border
    //Adds a border to each side of the z-stack. Size of the border
    is hard coded in the parameter section at the top.
    function addBorder(size, slice){

    file = getTitle();
    fileName = File.nameWithoutExtension;
    width = getWidth();
    height = getHeight();

    run("Canvas Size...", "width="+(width+(size*2))+"
    height="+(height+(size*2))+" position=Center zero");

    setBatchMode(true);
    for (i = 0; i < slice; i++) {

    run("Add Slice", "add=slice prepend");

    }

    for (i = 0; i < slice; i++) {
    setSlice(nSlices);
    run("Add Slice", "add=slice");

    }
    setBatchMode(false);


    }

    //Get points for midline
    //Creates a dialog to ask user to select 3 points on the midline
    to define the midline plane
    function getMidlinePoints(slice){
    do {
    setSlice(3*slice+30);
    run("Clear Results");
    run("Select None");
    Dialog.createNonBlocking("Define midline");
    setTool("multipoint");
    Dialog.addMessage("Use multipoint tool to select 3 points on the
    midline.\nEach point on a different slice at differnt heights.
    Preferably more than 5 slices apart.\n \nAlt-click or command-
    click to delete a selection\nClick \"OK\" after selecting 3
    points");
    Dialog.show();
```

```
run("Measure");
if (nResults == 3){

}
else{
     Dialog.create("Error");
     Dialog.addMessage("Incorrect number of points
selected.\nPlease try again.");
     Dialog.show();
}

} while (nResults != 3);


}


//Calculate and apply rotation
//Parses coordinates of the user defined points then calculates
and applies the required rotational transformations
function rotate() {
x1 = getResult("X", 0);
x2 = getResult("X", 1);
x3 = getResult("X", 2);
y1 = getResult("Y", 0);
y2 = getResult("Y", 1);
y3 = getResult("Y", 2);
z1 = getResult("Slice", 0);
z2 = getResult("Slice", 1);
z3 = getResult("Slice", 2);



     //define vectors
vectorABi = x2-x1;
vectorABj = y2-y1;
vectorABk = z2-z1;

vectorACi = x3-x1;
vectorACj = y3-y1;
vectorACk = z3-z1;

     //ABxAC
A = (vectorABj*vectorACk)-(vectorABk*vectorACj);
B = (vectorABk*vectorACi)-(vectorABi*vectorACk);
C = (vectorABi*vectorACj)-(vectorABj*vectorACi);
D = -(A*x1+B*y1+C*z1);


     //rotation angles
yAxis = 180/PI*atan(C/A);
```

```
zAxis = -180/PI*atan(B/A);

run("TransformJ Rotate", "z-angle="+zAxis+" y-angle="+yAxis+" x-
angle=0.0 interpolation=Linear background=0.0");

}

//Calculate translation
//Determines midline position after rotation and translates image
along the x-axis to position the midline at the location defined
by the midlinePixel parameter
function translateMidline() {
do {
run("Select None");
setSlice(nSlices/2);
Dialog.createNonBlocking("Define midline");
setTool("line");
Dialog.addMessage("Hold shift and draw line on midline\nClick
\"ok\" when ready")
Dialog.show();
getLine(a1, b1, a2, b2, lineWidth);

if (a1 == -1) {
Dialog.create("Error");
Dialog.addMessage("No line selected");
Dialog.show();
}

if (a1 != a2) {
Dialog.create("Error");
Dialog.addMessage("Line not vertical.\n \nMake sure to hold shift
when drawing line");
Dialog.show();

a1 = -1;
}

} while (a1 == -1);
translate = midlinePixel-a1;

run("TransformJ Translate", "x-distance="+translate+" y-
distance=0.0 z-distance=0.0 voxel interpolation=Linear
background=0.0");
}
```

## References

Almeida, M.P., Welker, J.M., Siddiqui, S., Luiken, J., Ekker, S.C., Clark, K.J., Essner, J.J., and McGrail, M. (2021). Endogenous zebrafish proneural Cre drivers generated by CRISPR/Cas9 short homology directed targeted integration. Sci. Rep. *11*, 1732.

Armit, C., Richardson, L., Venkataraman, S., Graham, L., Burton, N., Hill, B., Yang, Y., and Baldock, R.A. (2017). eMouseAtlas: An atlas-based resource for understanding mammalian embryogenesis. Dev. Biol. *423*, 1–11.

Assens, A., Dal Col, J.A., Njoku, A., Dietschi, Q., Kan, C., Feinstein, P., Carleton, A., and Rodriguez, I. (2016). Alteration of Nrp1 signaling at different stages of olfactory neuron maturation promotes glomerular shifts along distinct axes in the olfactory bulb. Development *143*, 3817–3825.

Astic, L., Saucier, D., and Holley, A. (1987). Topographical relationships between olfactory receptor cells and glomerular foci in the rat olfactory bulb. Brain Res. *424*, 144–152.

Avants, B.B., Yushkevich, P., Pluta, J., Minkoff, D., Korczykowski, M., Detre, J., and Gee, J.C. (2009). The optimal template effect in hippocampus studies of diseased populations. Neuroimage *49*, 2457–2466.

Bargmann, C.I., and Horvitz, H.R. (1991). Chemosensory neurons with overlapping functions direct chemotaxis to multiple chemicals in C. elegans. Neuron *7*, 729–742.

Barth, A.L., Justice, N.J., and Ngai, J. (1996). Asynchronous onset of odorant receptor expression in the developing zebrafish olfactory system. Neuron *16*, 23–34.

Barth, A.L., Dugas, J.C., and Ngai, J. (1997). Noncoordinate expression of odorant receptor genes tightly linked in the zebrafish genome. Neuron *19*, 359–369.

Baum, M.J., and Kelliher, K.R. (2009). Complementary roles of the main and accessory olfactory systems in mammalian mate recognition. Annu. Rev. Physiol. *71*, 141–160.

Bayramli, X., Kocagöz, Y., Sakizli, U., and Fuss, S.H. (2017). Patterned Arrangements of Olfactory Receptor Gene Expression in Zebrafish are Established by Radial Movement of Specified Olfactory Sensory Neurons. Sci. Rep. *7*.

Belluscio, L., Koentges, G., Axel, R., and Dulac, C. (1999). A map of pheromone receptor activation in the mammalian brain. Cell *97*, 209–220.

Boehm, U., Zou, Z., and Buck, L.B. (2005). Feedback loops link odor and pheromone signaling with reproduction. Cell *123*, 683–695.

Braubach, O.R., Miyasaka, N., Koide, T., Yoshihara, Y., Croll, R.P., and Fine, A. (2013). Experience-dependent versus experience-independent postembryonic development of distinct groups of zebrafish olfactory glomeruli. J. Neurosci. *33*, 6905–6916.

Brend, T., and Holley, S.A. (2009). Zebrafish whole mount high-resolution double fluorescent in situ hybridization. J. Vis. Exp.

Brennan, P.A., and Zufall, F. (2006). Pheromonal communication in vertebrates. Nature *444*, 308–315.

Brose, K., and Tessier-Lavigne, M. (2000). Slit proteins: key regulators of axon guidance, axonal branching, and cell migration. Curr. Opin. Neurobiol. *10*, 95–102.

Buck, L., and Axel, R. (1991). A novel multigene family may encode odorant receptors: a molecular basis for odor recognition. Cell *65*, 175–187.

Bundschuh, S.T., Zhu, P., Scharer, Y.-P.Z., and Friedrich, R.W. (2012). Dopaminergic Modulation of Mitral Cells and Odor Responses in the Zebrafish Olfactory Bulb. J. Neurosci. *32*, 6830–6840.

Bushdid, C., Magnasco, M.O., Vosshall, L.B., and Keller, A. (2014). Humans Can Discriminate More than 1 Trillion Olfactory Stimuli. Science (80-. ). *343*, 1370–1372.

Chalasani, S.H., Sabol, A., Xu, H., Gyda, M.A., Rasband, K., Granato, M., Chien, C.-B., and Raper, J.A. (2007). Stromal Cell-Derived Factor-1 Antagonizes Slit/Robo Signaling In Vivo. J. Neurosci. *27*, 973–980.

Chen, H., Chédotal, A., He, Z., Goodman, C.S., and Tessier-Lavigne, M. (1997). Neuropilin-2, a novel member of the neuropilin family, is a high affinity receptor for the semaphorins Sema E and Sema IV but not Sema III. Neuron *19*, 547–559.

Chen, H., He, Z., Bagri, A., and Tessier-Lavigne, M. (1998). Semaphorin-neuropilin interactions underlying sympathetic axon responses to class III semaphorins. Neuron *21*, 1283–1290.

Cheng, R.P., Dang, P., Taku, A.A., Moon, Y.J., Pham, V., Sun, X., Zhao, E., and Raper, J.A. (2022). Loss of Neuropilin2a/b or Sema3fa alters olfactory sensory axon dynamics and protoglomerular targeting. Neural Dev. *17*, 1.

Cho, J.H., Lepine, M., Andrews, W., Parnavelas, J., and Cloutier, J.-F. (2007). Requirement for Slit-1 and Robo-2 in Zonal Segregation of Olfactory Sensory Neuron Axons in the Main Olfactory Bulb. J. Neurosci. *27*, 9094–9104.

Cho, J.H., Prince, J.E.A., Cutforth, T., and Cloutier, J.-F. (2011). The pattern of glomerular map formation defines responsiveness to aversive odorants in mice. J. Neurosci. *31*, 7920–7926.

Cho, J.H., Kam, J.W.K., and Cloutier, J.F. (2012). Slits and Robo-2 regulate the coalescence of subsets of olfactory sensory neuron axons within the ventral region of the olfactory bulb. Dev. Biol. *371*, 269–279.

Clark, K.J., Balciunas, D., Pogoda, H.-M., Ding, Y., Westcot, S.E., Bedell, V.M., Greenwood, T.M., Urban, M.D., Skuster, K.J., Petzold, A.M., et al. (2011). In vivo protein trapping produces a functional expression codex of the vertebrate proteome. Nat. Methods *8*, 506–512.

Cloutier, J.-F., Giger, R.J., Koentges, G., Dulac, C., Kolodkin, A.L., and Ginty, D.D. (2002). Neuropilin-2 Mediates Axonal Fasciculation, Zonal Segregation, but Not Axonal

Convergence, of Primary Accessory Olfactory Neurons. Neuron *33*, 877–892.

Cloutier, J.F., Sahay, A., Chang, E.C., Tessier-Lavigne, M., Dulac, C., Kolodkin, A.L., and Ginty, D.D. (2004). Differential requirements for semaphorin 3F and slit-1 in axonal targeting, fasciculation, and segregation of olfactory sensory neuron projections. J. Neurosci. *24*, 9087–9096.

Comer, J.D., Alvarez, S., Butler, S.J., and Kaltschmidt, J.A. (2019). Commissural axon guidance in the developing spinal cord: from Cajal to the present day. Neural Dev. *14*, 9.

Dang, P., Fisher, S.A., Stefanik, D.J., Kim, J., and Raper, J.A. (2018). Coordination of olfactory receptor choice with guidance receptor expression and function in olfactory sensory neurons. PLoS Genet. *14*, e1007164.

DeMaria, S., Berke, A.P., Van Name, E., Heravian, A., Ferreira, T., and Ngai, J. (2013). Role of a Ubiquitously Expressed Receptor in the Vertebrate Olfactory System. J. Neurosci. *33*, 15235–15247.

Dieris, M., Ahuja, G., Krishna, V., and Korsching, S.I. (2017). A single identified glomerulus in the zebrafish olfactory bulb carries the high-affinity response to death-associated odor cadaverine. Sci. Rep. *7*, 40892.

Dobin, A., Davis, C.A., Schlesinger, F., Drenkow, J., Zaleski, C., Jha, S., Batut, P., Chaisson, M., and Gingeras, T.R. (2013). STAR: ultrafast universal RNA-seq aligner. Bioinformatics *29*, 15–21.

Dulac, C. (2000). Sensory coding of pheromone signals in mammals. Curr. Opin. Neurobiol. *10*, 511–518.

Dulac, C., and Axel, R. (1995). A novel family of genes encoding putative pheromone receptors in mammals. Cell *83*, 195–206.

Dynes, J.L., and Ngai, J. (1998). Pathfinding of olfactory neuron axons to stereotyped glomerular targets revealed by dynamic imaging in living zebrafish embryos. Neuron *20*, 1081–1091.

Edison, A.S. (2009). Caenorhabditis elegans pheromones regulate multiple complex behaviors. Curr. Opin. Neurobiol. *19*, 378–388.

Feng, B., Bulchand, S., Yaksi, E., Friedrich, R.W., and Jesuthasan, S. (2005). The recombination activation gene 1 (Rag1) is expressed in a subset of zebrafish olfactory neurons but is not essential for axon targeting or amino acid detection. BMC Neurosci. *6*, 46.

Fernandez, R., and Moisy, C. (2021). Fijiyama: a registration tool for 3D multimodal time-lapse imaging. Bioinformatics *37*, 1482–1484.

Friedrich, R.W., and Korsching, S.I. (1997). Combinatorial and chemotopic odorant coding in the zebrafish olfactory bulb visualized by optical imaging. Neuron *18*, 737–752.

Friedrich, R.W., and Korsching, S.I. (1998). Representations in the Olfactory Bulb Revealed Using a Voltage-Sensitive Axon Tracer. J. Neurosci. *18*, 9977–9988.

Gagnon, J. a., Valen, E., Thyme, S.B., Huang, P., Akhmetova, L., Ahkmetova, L., Pauli, A., Montague, T.G., Zimmerman, S., Richter, C., et al. (2014). Efficient mutagenesis by Cas9 protein-mediated oligonucleotide insertion and large-scale assessment of single-guide RNAs. PLoS One *9*, e98186.

Gerkin, R.C., and Castro, J.B. (2015). The number of olfactory stimuli that humans can discriminate is still unknown. Elife *4*, e08127.

Glasauer, S.M.K., and Neuhauss, S.C.F. (2014). Whole-genome duplication in teleost fishes and its evolutionary consequences. Mol. Genet. Genomics *289*, 1045–1060.

Godinho, L. (2011). Imaging zebrafish development. Cold Spring Harb. Protoc. *2011*, 879–883.

Ha, T.S., and Smith, D.P. (2009). Odorant and pheromone receptors in insects. Front. Cell. Neurosci. *3*, 1–6.

Halpern, M. (1987). The Organization and Function of the Vomeronasal System. Annu. Rev. Neurosci. *10*, 325–362.

He, Z., Crenshaw, E., and Raper, J.A. (2019). Semaphorin/neuropilin binding specificities are stable over 400 million years of evolution. Biochem. Biophys. Res. Commun. *517*, 23–28.

Heimbeck, G., Bugnon, V., Gendre, N., Keller, A., and Stocker, R.F. (2001). A central neural circuit for experience-independent olfactory and courtship behavior in Drosophila melanogaster. Proc. Natl. Acad. Sci. U. S. A. *98*, 15336–15341.

Herrera, K.J., Panier, T., Guggiana-Nilo, D., and Engert, F. (2021). Larval Zebrafish Use Olfactory Detection of Sodium and Chloride to Avoid Salt Water. Curr. Biol. 1–12.

Hong, W., and Luo, L. (2014). Genetic control of wiring specificity in the fly olfactory system. Genetics *196*, 17–29.

Hoover, K.C. (2010). Smell with inspiration: The evolutionary significance of olfaction. Am. J. Phys. Anthropol. *143*, 63–74.

van Horck, F.P.G., Weinl, C., and Holt, C.E. (2004). Retinal axon guidance: novel mechanisms for steering. Curr. Opin. Neurobiol. *14*, 61–66.

Hussain, A., Saraiva, L.R., Ferrero, D.M., Ahuja, G., Krishna, V.S., Liberles, S.D., and Korsching, S.I. (2013). High-affinity olfactory receptor for the death-associated odor cadaverine. Proc. Natl. Acad. Sci.

Hwang, W.Y., Fu, Y., Reyon, D., Maeder, M.L., Tsai, S.Q., Sander, J.D., Peterson, R.T., Yeh, J.-R.R.J.J., and Joung, J.K. (2013). Efficient genome editing in zebrafish using a CRISPR-Cas system. Nat. Biotechnol. *31*, 227–229.

Imai, T., Suzuki, M., and Sakano, H. (2006). Odorant Receptor–Derived cAMP Signals Direct Axonal Targeting. Science (80-. ). *314*, 657–661.

Imai, T., Yamazaki, T., Kobayakawa, R., Kobayakawa, K., Abe, T., Suzuki, M., and

Sakano, H. (2009). Pre-target axon sorting establishes the neural map topography. Science (80-. ). *325*, 585–590.

Inokuchi, K., Imamura, F., Takeuchi, H., Kim, R., Okuno, H., Nishizumi, H., Bito, H., Kikusui, T., and Sakano, H. (2017). Nrp2 is sufficient to instruct circuit formation of mitral-cells to mediate odour-induced attractive social responses. Nat. Commun. *8*, 15977.

Jefferis, G.S.X.E., Potter, C.J., Chan, A.M., Marin, E.C., Rohlfing, T., Maurer, C.R., and Luo, L. (2007). Comprehensive Maps of Drosophila Higher Olfactory Centers: Spatially Segregated Fruit and Pheromone Representation. Cell *128*, 1187–1203.

Jeong, Y.M., Choi, T.I., Hwang, K.S., Lee, J.S., Gerlai, R., and Kim, C.H. (2021). Optogenetic manipulation of olfactory responses in transgenic zebrafish: A neurobiological and behavioral study. Int. J. Mol. Sci. *22*.

Joo, W.J., Sweeney, L.B., Liang, L., and Luo, L. (2013). Linking cell fate, trajectory choice, and target selection: Genetic analysis of sema-2b in olfactory axon targeting. Neuron *78*, 673–686.

Kalafatakis, I., Kalafatakis, K., Tsimpolis, A., Giannakeas, N., Tsipouras, M., Tzallas, A., and Karagogeos, D. (2020). Using the Allen gene expression atlas of the adult mouse brain to gain further insight into the physiological significance of TAG-1/Contactin-2. Brain Struct. Funct. *225*, 2045–2056.

Kang, N., Baum, M.J., and Cherry, J.A. (2011). Different profiles of main and accessory olfactory bulb mitral/tufted cell projections revealed in mice using an anterograde tracer and a whole-mount, flattened cortex preparation. Chem. Senses *36*, 251–260.

Keller, M., Baum, M.J., Brock, O., Brennan, P.A., and Bakker, J. (2009). The main and the accessory olfactory systems interact in the control of mate recognition and sexual behavior. Behav. Brain Res. *200*, 268–276.

Kennedy, T.E. (2000a). Cellular mechanisms of netrin function: long-range and short-range actions. Biochem. Cell Biol. *78*, 569–575.

Kennedy, T.E. (2000b). Cellular mechanisms of netrin function: long-range and short-range actions. Biochem. Cell Biol. *78*, 569–575.

Kermen, F., Darnet, L., Wiest, C., Palumbo, F., Bechert, J., Uslu, O., and Yaksi, E. (2020). Stimulus-specific behavioral responses of zebrafish to a large range of odors exhibit individual variability. BMC Biol. *18*, 66.

Kimmel, C.B., Ballard, W.W., Kimmel, S.R., Ullmann, B., and Schilling, T.F. (1995). Stages of embryonic development of the zebrafish. Dev. Dyn. *203*, 253–310.

Knöll, B., Zarbalis, K., Wurst, W., and Drescher, U. (2001). A role for the EphA family in the topographic targeting of vomeronasal axons. Development *128*, 895–906.

Knöll, B., Schmidt, H., Andrews, W., Guthrie, S., Pini, A., Sundaresan, V., and Drescher, U. (2003). On the topographic targeting of basal vomeronasal axons through Slit-

mediated chemorepulsion. Development *130*, 5073–5082.

Koide, T., Miyasaka, N., Morimoto, K., Asakawa, K., Urasaki, A., Kawakami, K., and Yoshihara, Y. (2009). Olfactory neural circuitry for attraction to amino acids revealed by transposon-mediated gene trap approach in zebrafish. Proc. Natl. Acad. Sci. U. S. A. *106*, 9884–9889.

Komiyama, T., Sweeney, L.B., Schuldiner, O., Garcia, K.C., and Luo, L. (2007). Graded Expression of Semaphorin-1a Cell-Autonomously Directs Dendritic Targeting of Olfactory Projection Neurons. Cell *128*, 399–410.

Kunst, M., Laurell, E., Mokayes, N., Kramer, A., Kubo, F., Fernandes, A.M., Förster, D., Dal Maschio, M., and Baier, H. (2019). A Cellular-Resolution Atlas of the Larval Zebrafish Brain. Neuron *103*, 21-38.e5.

Lakhina, V., Marcaccio, C.L., Shao, X., Lush, M.E., Jain, R. a., Fujimoto, E., Bonkowsky, J.L., Granato, M., and Raper, J. a. (2012). Netrin/DCC Signaling Guides Olfactory Sensory Axons to Their Correct Location in the Olfactory Bulb. J. Neurosci. *32*, 4440–4456.

Li, J., Mack, J. a, Souren, M., Yaksi, E., Higashijima, S., Mione, M., Fetcho, J.R., and Friedrich, R.W. (2005). Early development of functional spatial maps in the zebrafish olfactory bulb. J. Neurosci. *25*, 5784–5795.

Lindsay, S.M., and Vogt, R.G. (2004). Behavioral responses of newly hatched zebrafish (Danio rerio) to amino acid chemostimulants. Chem. Senses *29*, 93–100.

Lipschitz, D.L., and Michel, W.C. (2002). Amino acid odorants stimulate microvillar sensory neurons. Chem. Senses *27*, 277–286.

Love, M.I., Huber, W., and Anders, S. (2014). Moderated estimation of fold change and dispersion for RNA-seq data with DESeq2. Genome Biol. *15*, 550.

Luu, P., Acher, F., Bertrand, H.O., Fan, J., and Ngai, J. (2004). Molecular determinants of ligand selectivity in a vertebrate odorant receptor. J. Neurosci. *24*, 10128–10137.

Macosko, E.Z., Pokala, N., Feinberg, E.H., Chalasani, S.H., Butcher, R.A., Clardy, J., and Bargmann, C.I. (2009). A hub-and-spoke circuit drives pheromone attraction and social behaviour in C. elegans. Nature *458*, 1171–1175.

Malnic, B., Hirono, J., Sato, T., and Buck, L.B. (1999). Combinatorial receptor codes for odors. Cell *96*, 713–723.

Mayhew, E.J., Arayata, C.J., Gerkin, R.C., Lee, B.K., Magill, J.M., Snyder, L.L., Little, K.A., Yu, C.W., and Mainland, J.D. (2021). Drawing the Borders of Olfactory Space. BioRxiv 2020.12.04.412254.

Meister, M. (2015). On the dimensionality of odor space. Elife *4*, e07865.

Miyamichi, K., Serizawa, S., Kimura, H.M., and Sakano, H. (2005). Continuous and overlapping expression domains of odorant receptor genes in the olfactory epithelium determine the dorsal/ventral positioning of glomeruli in the olfactory bulb. J. Neurosci.

*25*, 3586–3592.

Miyasaka, N., Sato, Y., Yeo, S.-Y., Hutson, L.D., Chien, C.-B., Okamoto, H., and Yoshihara, Y. (2005). Robo2 is required for establishment of a precise glomerular map in the zebrafish olfactory system. Development *132*, 1283–1293.

Miyasaka, N., Morimoto, K., Tsubokawa, T., Higashijima, S.I., Okamoto, H., and Yoshihara, Y. (2009). From the olfactory bulb to higher brain Centers: Genetic visualization of secondary olfactory pathways in zebrafish. J. Neurosci. *29*, 4756–4767.

Miyasaka, N., Arganda-Carreras, I., Wakisaka, N., Masuda, M., Sümbül, U., Seung, H.S., and Yoshihara, Y. (2014). Olfactory projectome in the zebrafish forebrain revealed by genetic single-neuron labelling. Nat. Commun. *5*, 3639.

Montague, T.G., Jos´, J., Cruz, J.M., Gagnon, J.A., Church, G.M., and Valen, E. (2014). CHOPCHOP: A CRISPR/Cas9 and TALEN web tool for genome editing. Nucleic Acids Res. *42*, 401–407.

Morris, J., Singh, J.M., and Eberwine, J.H. (2011). Transcriptome Analysis of Single Cells. J. Vis. Exp. e2634.

Mosimann, C., Kaufman, C.K., Li, P., Pugach, E.K., Tamplin, O.J., and Zon, L.I. (2011). Ubiquitous transgene expression and Cre-based recombination driven by the ubiquitin promoter in zebrafish. Development *138*, 169–177.

Mosimann, C., Puller, A.C., Lawson, K.L., Tschopp, P., Amsterdam, A., and Zon, L.I. (2013). Site-directed zebrafish transgenesis into single landing sites with the phiC31 integrase system. Dev. Dyn. *242*, 949–963.

Mullins, M.C., Hammerschmidt, M., Haffter, P., and Nüsslein-Volhard, C. (1994). Large-scale mutagenesis in the zebrafish: in search of genes controlling development in a vertebrate. Curr. Biol. *4*, 189–202.

Nakashima, A., Takeuchi, H., Imai, T., Saito, H., Kiyonari, H., Abe, T., Chen, M., Weinstein, L.S., Yu, C.R., Storm, D.R., et al. (2013). XAgonist-independent GPCR activity regulates anterior-posterior targeting of olfactory sensory neurons. Cell *154*, 1314–1325.

Nakashima, A., Ihara, N., Shigeta, M., Kiyonari, H., Ikegaya, Y., and Takeuchi, H. (2019). Structured spike series specify gene expression patterns for olfactory circuit formation. Science (80-. ). *364*.

Ngai, J., Chess, A., Dowling, M.M., Necles, N., Macagno, E.R., and Axel, R. (1993). Coding of olfactory information: Topography of odorant receptor expression in the catfish olfactory epithelium. Cell *72*, 667–680.

Nguyen-Ba-Charvet, K.T., Di Meglio, T., Fouquet, C., and Chédotal, A. (2008). Robos and slits control the pathfinding and targeting of mouse olfactory sensory axons. J. Neurosci. *28*, 4244–4249.

Nishizumi, H., and Sakano, H. (2015). Developmental regulation of neural map formation

in the mouse olfactory system. Dev. Neurobiol. *75*, 594–607.

Norlin, E.M., Alenius, M., Gussing, F., Hägglund, M., Vedin, V., and Bohm, S. (2001). Evidence for gradients of gene expression correlating with zonal topography of the olfactory sensory map. Mol. Cell. Neurosci. *18*, 283–295.

Olender, T., Jones, T.E.M., Bruford, E., and Lancet, D. (2020). A unified nomenclature for vertebrate olfactory receptors. BMC Evol. Biol. *20*, 42.

Prince, J.E.A., Cho, J.H., Dumontier, E., Andrews, W., Cutforth, T., Tessier-Lavigne, M., Parnavelas, J., and Cloutier, J.-F. (2009). Robo-2 controls the segregation of a portion of basal vomeronasal sensory neuron axons to the posterior region of the accessory olfactory bulb. J. Neurosci. *29*, 14211–14222.

Prince, J.E.A., Brignall, A.C., Cutforth, T., Shen, K., and Cloutier, J.-F. (2013). Kirrel3 is required for the coalescence of vomeronasal sensory neuron axons into glomeruli and for male-male aggression. Development *140*, 2398–2408.

Ressler, K.J., Sullivan, S.L., and Buck, L.B. (1993). A zonal organization of odorant receptor gene expression in the olfactory epithelium. Cell *73*, 597–609.

Ressler, K.J., Sullivan, S.L., and Buck, L.B. (1994). Information coding in the olfactory system: Evidence for a stereotyped and highly organized epitope map in the olfactory bulb. Cell *79*, 1245–1255.

Richardson, L., Venkataraman, S., Stevenson, P., Yang, Y., Moss, J., Graham, L., Burton, N., Hill, B., Rao, J., Baldock, R.A., et al. (2014). EMAGE mouse embryo spatial gene expression database: 2014 update. Nucleic Acids Res. *42*, D835–D844.

Rodriguez, I., Feinstein, P., and Mombaerts, P. (1999). Variable patterns of axonal projections of sensory neurons in the mouse vomeronasal system. Cell *97*, 199–208.

Ronneberger, O., Liu, K., Rath, M., Rueβ, D., Mueller, T., Skibbe, H., Drayer, B., Schmidt, T., Filippi, A., Nitschke, R., et al. (2012). ViBE-Z: a framework for 3D virtual colocalization analysis in zebrafish larval brains. Nat. Methods *9*, 735–742.

Ruta, V., Datta, S.R., Vasconcelos, M.L., Freeland, J., Looger, L.L., and Axel, R. (2010). A dimorphic pheromone circuit in Drosophila from sensory input to descending output. Nature *468*, 686–690.

Sakano, H. (2010). Neural map formation in the mouse olfactory system. Neuron *67*, 530–542.

Sato, Y., Miyasaka, N., and Yoshihara, Y. (2005). Mutually exclusive glomerular innervation by two distinct types of olfactory sensory neurons revealed in transgenic zebrafish. J. Neurosci. *25*, 4889–4897.

Sato, Y., Miyasaka, N., and Yoshihara, Y. (2007). Hierarchical regulation of odorant receptor gene choice and subsequent axonal projection of olfactory sensory neurons in zebrafish. J. Neurosci. *27*, 1606–1615.

Schaefer, M.L., Finger, T.E., and Restrepo, D. (2001). Variability of position of the P2

glomerulus within a map of the mouse olfactory bulb. J. Comp. Neurol. *436*, 351–362.

Schwarting, G.A., Kostek, C., Ahmad, N., Dibble, C., Pays, L., and Püschel, A.W. (2000). Semaphorin 3A is required for guidance of olfactory axons in mice. J. Neurosci. *20*, 7691–7697.

Serizawa, S., Miyamichi, K., Takeuchi, H., Yamagishi, Y., Suzuki, M., and Sakano, H. (2006). A Neuronal Identity Code for the Odorant Receptor-Specific and Activity-Dependent Axon Sorting. Cell *127*, 1057–1069.

Shao, X., Lakhina, V., Dang, P., Cheng, R.P., Marcaccio, C.L., and Raper, J.A. (2017). Olfactory sensory axons target specific protoglomeruli in the olfactory bulb of zebrafish. Neural Dev. *12*, 18.

Sharma, A., Verhaagen, J., and Harvey, A.R. (2012). Receptor complexes for each of the class 3 Semaphorins. Front. Cell. Neurosci. *6*, 1–13.

Stephan, A.B., Shum, E.Y., Hirsh, S., Cygnar, K.D., Reisert, J., and Zhao, H. (2009). ANO2 is the cilial calcium-activated chloride channel that may mediate olfactory amplification. Proc. Natl. Acad. Sci. U. S. A. *106*, 11776–11781.

Stettler, D.D., and Axel, R. (2009). Representations of odor in the piriform cortex. Neuron *63*, 854–864.

Stowers, L., Cameron, P., and Keller, J.A. (2013). Ominous odors: Olfactory control of instinctive fear and aggression in mice. Curr. Opin. Neurobiol. *23*, 339–345.

Strotmann, J., Conzelmann, S., Beck, a, Feinstein, P., Breer, H., and Mombaerts, P. (2000). Local permutations in the glomerular array of the mouse olfactory bulb. J. Neurosci. *20*, 6927–6938.

Suárez, R., García-González, D., and de Castro, F. (2012). Mutual influences between the main olfactory and vomeronasal systems in development and evolution. Front. Neuroanat. *6*, 1–14.

Sullivan, S.L., Bohm, S., Ressler, K.J., Horowitz, L.F., and Buck, L.B. (1995). Target-independent pattern specification in the olfactory epithelium. Neuron *15*, 779–789.

Sweeney, L.B., Chou, Y.H., Wu, Z., Joo, W., Komiyama, T., Potter, C.J., Kolodkin, A.L., Garcia, K.C., and Luo, L. (2011). Secreted semaphorins from degenerating larval ORN axons direct adult projection neuron dendrite targeting. Neuron *72*, 734–747.

Takeuchi, H., Inokuchi, K., Aoki, M., Suto, F., Tsuboi, A., Matsuda, I., Suzuki, M., Aiba, A., Serizawa, S., Yoshihara, Y., et al. (2010). Sequential Arrival and Graded Secretion of Sema3F by Olfactory Neuron Axons Specify Map Topography at the Bulb. Cell *141*, 1056–1067.

Taku, A.A., Marcaccio, C.L., Ye, W., Krause, G.J., and Raper, J.A. (2016). Attractant and repellent cues cooperate in guiding a subset of olfactory sensory axons to a well-defined protoglomerular target. Dev. *143*, 123–132.

Taniguchi, M., Nagao, H., Takahashi, Y.K., Yamaguchi, M., Mitsui, S., Yagi, T., Mori, K.,

and Shimizu, T. (2003). Distorted odor maps in the olfactory bulb of semaphorin 3A-deficient mice. J. Neurosci. *23*, 1390–1397.

Vaddadi, N., Iversen, K., Raja, R., Phen, A., Brignall, A., Dumontier, E., and Cloutier, J.-F. (2019). Kirrel2 is differentially required in populations of olfactory sensory neurons for the targeting of axons in the olfactory bulb. Development *146*.

Vassar, R., Ngai, J., and Axel, R. (1993). Spatial segregation of odorant receptor expression in the mammalian olfactory epithelium. Cell *74*, 309–318.

Vassar, R., Chao, S.K., Sitcheran, R., Nuñez, J.M., Vosshall, L.B., and Axel, R. (1994). Topographic organization of sensory projections to the olfactory bulb. Cell *79*, 981–991.

Wachowiak, M., and Cohen, L.B. (2001). Representation of odorants by receptor neuron input to the mouse olfactory bulb. Neuron *32*, 723–735.

Wagner, S., Gresser, A.L., Torello, A.T., and Dulac, C. (2006). A multireceptor genetic approach uncovers an ordered integration of VNO sensory inputs in the accessory olfactory bulb. Neuron *50*, 697–709.

Wakisaka, N., Miyasaka, N., Koide, T., Masuda, M., Hiraki-Kajiyama, T., and Yoshihara, Y. (2017). An Adenosine Receptor for Olfaction in Fish. Curr. Biol. *27*, 1437-1447.e4.

Walz, A., Rodriguez, I., and Mombaerts, P. (2002). Aberrant Sensory Innervation of the Olfactory Bulb in Neuropilin-2 Mutant Mice. J. Neurosci. *22*, 4025–4035.

Wang, F., Nemes, A., Mendelsohn, M., and Axel, R. (1998). Odorant Receptors Govern the Formation of a Precise Topographic Map. Cell *93*, 47–60.

Weiss, L., Jungblut, L.D., Pozzi, A.G., Zielinski, B.S., O'Connell, L.A., Hassenklöver, T., and Manzini, I. (2020). Multi-glomerular projection of single olfactory receptor neurons is conserved among amphibians. J. Comp. Neurol. 1–15.

Weth, F., Nadler, W., and Korsching, S. (1996). Nested expression domains for odorant receptors in zebrafish olfactory epithelium. Proc. Natl. Acad. Sci. U. S. A. *93*, 13321–13326.

Whitlock, K.E., and Westerfield, M. (1998). A Transient Population of Neurons Pioneers the Olfactory Pathway in the Zebrafish. J. Neurosci. *18*, 8919–8927.

Wong, S.T., Trinh, K., Hacker, B., Chan, G.C., Lowe, G., Gaggar, A., Xia, Z., Gold, G.H., and Storm, D.R. (2000). Disruption of the type III adenylyl cyclase gene leads to peripheral and behavioral anosmia in transgenic mice. Neuron *27*, 487–497.

Yabuki, Y., Koide, T., Miyasaka, N., Wakisaka, N., Masuda, M., Ohkura, M., Nakai, J., Tsuge, K., Tsuchiya, S., Sugimoto, Y., et al. (2016). Olfactory receptor for prostaglandin F2α mediates male fish courtship behavior. Nat. Neurosci. *19*, 897–904.

Yemini, E., Lin, A., Nejatbakhsh, A., Varol, E., Sun, R., Mena, G.E., Samuel, A.D.T., Paninski, L., Venkatachalam, V., and Hobert, O. (2021). NeuroPAL: A Multicolor Atlas for Whole-Brain Neuronal Identification in C. elegans. Cell *184*, 272-288.e11.

Yu, H.-H., and Moens, C.B. (2005). Semaphorin signaling guides cranial neural crest cell migration in zebrafish. Dev. Biol. *280*, 373–385.

Yu, H.-H., Houart, C., and Moens, C.B. (2004). Cloning and embryonic expression of zebrafish neuropilin genes. Gene Expr. Patterns *4*, 371–378.

Zapiec, B., and Mombaerts, P. (2015). Multiplex assessment of the positions of odorant receptor-specific glomeruli in the mouse olfactory bulb by serial two-photon tomography. Proc. Natl. Acad. Sci. *112*, E5873-82.

Zapiec, B., and Mombaerts, P. (2020). The Zonal Organization of Odorant Receptor Gene Choice in the Main Olfactory Epithelium of the Mouse. Cell Rep. *30*, 4220-4234.e5.

Zapiec, B., Bressel, O.C., Khan, M., Walz, A., and Mombaerts, P. (2016). Neuropilin-1 and the Positions of Glomeruli in the Mouse Olfactory Bulb. Eneuro *3*, ENEURO.0123-16.2016.

Zhang, J., Huang, G., Dewan, A., Feinstein, P., and Bozza, T. (2012). Uncoupling stimulus specificity and glomerular position in the mouse olfactory system. Mol. Cell. Neurosci. *51*, 79–88.

Zhu, Q., Fisher, S.A., Shallcross, J., and Kim, J. (2016). VERSE: a versatile and efficient RNA-Seq read counting tool. BioRxiv 053306.